Article

Cell

Moderate UV Exposure Enhances Learning and Memory by Promoting a Novel Glutamate Biosynthetic Pathway in the Brain

Graphical Abstract

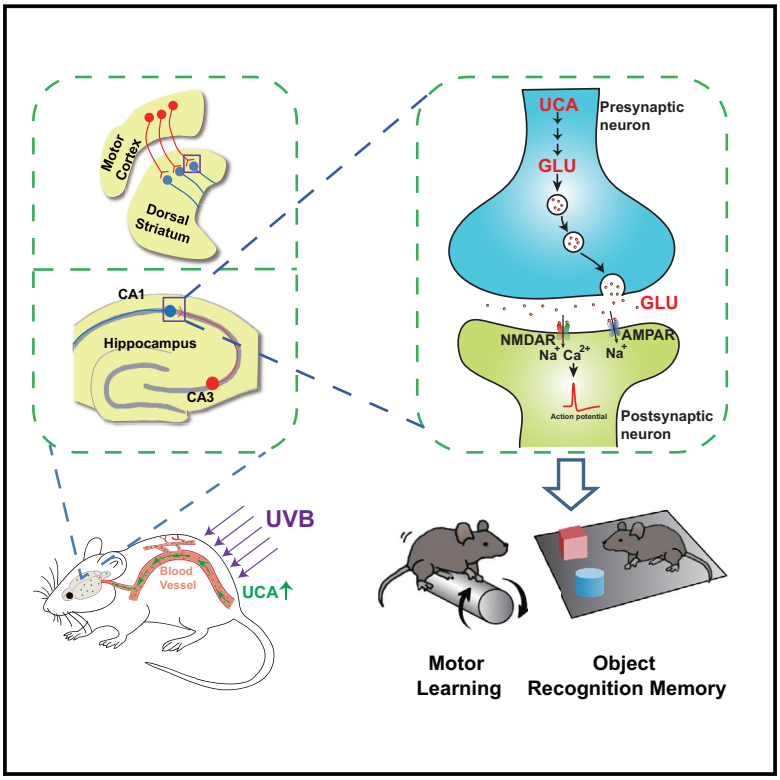

Authors

Hongying Zhu, Ning Wang, Lei Yao, ..., Xiaoyuan Song, Guangming Huang, Wei Xiong

Correspondence

gmhuang@ustc.edu.cn (G.H.), wxiong@ustc.edu.cn (W.X.)

In Brief

UV-induced upregulation of a small molecule feeds into an intraneuronal metabolic pathway for glutamate biosynthesis that can enhance learning and memory.

Highlights

- Single-cell mass spectrometry reveals a novel glutamate biosynthetic pathway in brain
- UV exposure leads to elevated blood and brain levels of urocanic acid in mice
- Urocanic acid promotes glutamate biosynthesis and release in various brain regions
- Moderate UV exposure improves motor learning and object recognition memory in mice

Zhu et al., 2018, Cell *173*, 1716–1727
June 14, 2018
https://doi.org/10.1016/j.cell.2018.04.014

CellPress

Cell

Article

Moderate UV Exposure Enhances Learning and Memory by Promoting a Novel Glutamate Biosynthetic Pathway in the Brain

Hongying Zhu,[1,3,6] Ning Wang,[1,6] Lei Yao,[1] Qi Chen,[1] Ran Zhang,[1] Junchao Qian,[4] Yiwen Hou,[1] Weiwei Guo,[1] Sijia Fan,[1] Siling Liu,[5] Qiaoyun Zhao,[1] Feng Du,[1] Xin Zuo,[1] Yujun Guo,[1] Yan Xu,[1] Jiali Li,[5] Tian Xue,[1,2] Kai Zhong,[2,4] Xiaoyuan Song,[1] Guangming Huang,[3,*] and Wei Xiong[1,2,7,*]

[1]Hefei National Laboratory for Physical Sciences at the Microscale, Neurodegenerative Disorder Research Center, School of Life Sciences, University of Science and Technology of China, 230026 Hefei, China

[2]Center for Excellence in Brain Science and Intelligence Technology, Chinese Academy of Sciences, 200031 Shanghai, China

[3]Hefei National Laboratory for Physical Sciences at the Microscale, School of Chemistry and Materials Science, University of Science and Technology of China, 230026 Hefei, China

[4]High Magnetic Field Laboratory, Chinese Academy of Sciences, 230031 Hefei, China

[5]Key Laboratory of Animal Models and Human Disease Mechanisms of Chinese Academy of Sciences & Yunnan Province, Kunming Institute of Zoology, Chinese Academy of Sciences, 650223 Kunming, China

[6]These authors contributed equally

[7]Lead Contact

*Correspondence: gmhuang@ustc.edu.cn (G.H.), wxiong@ustc.edu.cn (W.X.)

https://doi.org/10.1016/j.cell.2018.04.014

SUMMARY

Sunlight exposure is known to affect mood, learning, and cognition. However, the molecular and cellular mechanisms remain elusive. Here, we show that moderate UV exposure elevated blood urocanic acid (UCA), which then crossed the blood-brain barrier. Single-cell mass spectrometry and isotopic labeling revealed a novel intra-neuronal metabolic pathway converting UCA to glutamate (GLU) after UV exposure. This UV-triggered GLU synthesis promoted its packaging into synaptic vesicles and its release at glutamatergic terminals in the motor cortex and hippocampus. Related behaviors, like rotarod learning and object recognition memory, were enhanced after UV exposure. All UV-induced metabolic, electrophysiological, and behavioral effects could be reproduced by the intravenous injection of UCA and diminished by the application of inhibitor or short hairpin RNA (shRNA) against urocanase, an enzyme critical for the conversion of UCA to GLU. These findings reveal a new GLU biosynthetic pathway, which could contribute to some of the sunlight-induced neurobehavioral changes.

INTRODUCTION

Although UV exposure is associated with several skin diseases, moderate UV exposure is beneficial for human health. For example, UVB light, one form of radiant energy from sunlight, promotes vitamin D generation in the skin (Bouillon, 2017; Hart et al., 2011). UV radiation has been used to treat certain diseases, such as psoriasis, atopic dermatitis, eczema, cutaneous T cell lymphoma, vitiligo, and uremic pruritus (Ada et al., 2005; Archier et al., 2012; Johnson-Huang et al., 2010; Radack et al., 2015). Interestingly, UV light not only causes peripheral effects, but also is associated with various neurological behaviors linked to the CNS. Specifically, moderate UV exposure has been shown to affect mood, addiction, cognition, and memory (Beecher et al., 2016; Benedetti et al., 2001; Dominiak et al., 2015; Fell et al., 2014; Keller et al., 2005; Kent et al., 2009; Parrott and Sabini, 1990). However, relatively little is known about the molecular and cellular mechanisms that mediate UV-induced neurobehavioral changes.

Chronic UV exposure results in alterations in levels of proteins, peptides, and small molecules in the skin or blood, such as melanin, β-endorphin, vitamin D, and nitric oxide (Bouillon, 2017; D'Orazio et al., 2006; Fell et al., 2014; Hart et al., 2011; Holliman et al., 2017). Mounting evidence suggests that these peripheral changes in chemical substances in the blood induced by UV exposure may affect the brain. For example, UV exposure elevates skin β-endorphin, which may cross the blood-brain barrier (BBB), thus resulting in opioid-related antinociception and inducing addiction to UV light in mice (Fell et al., 2014). This finding suggests a connection between UV light-induced peripheral changes in circulating substances in the blood stream and brain function. In addition, levels of a small molecule called urocanic acid (UCA) in both epidermis and plasma have been found to increase immediately after UV exposure (Baden and Pathak, 1967; Kammeyer et al., 1997; Ruegemer et al., 2002). This compound absorbs UV light and thus confers UV ray-resistance (Barresi et al., 2011; Gibbs et al., 2008; Kammeyer et al., 1997; Ruegemer et al., 2002). The biological effects of elevated UCA in blood on the human body, particularly on brain function, have not been reported. Overall, it remains challenging to link UV exposure-induced alterations in the small molecules levels in the blood with their changes in the brain, owing to the lack of appropriate technical support for the sensitive and accurate

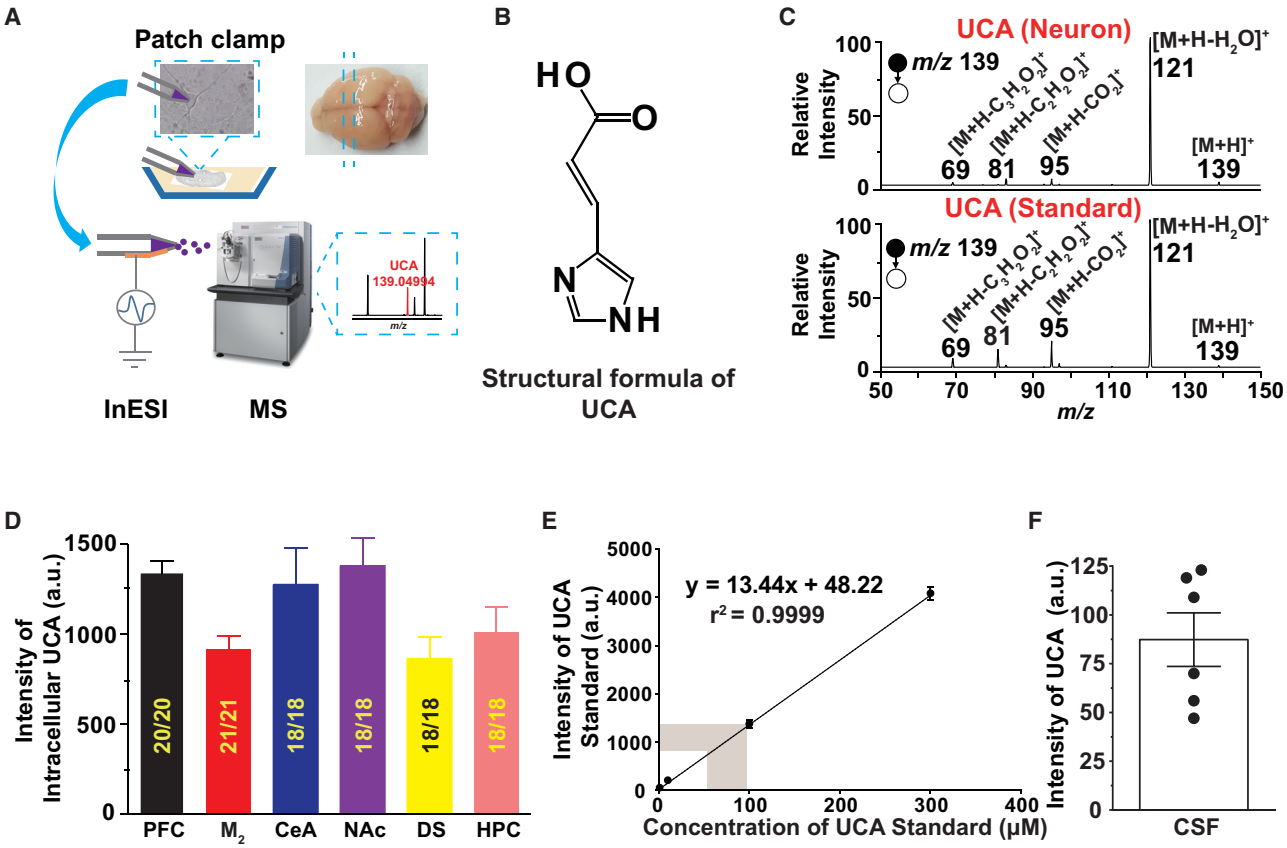

Figure 1. Identification of UCA in Neurons by Using Single-Cell MS

(A) Schematic of single-neuron MS. The expanded view depicts the mass spectra of UCA in single HPC neurons.

(B) Chemical structure of UCA.

(C) MS/MS to identify UCA in single HPC neurons and the UCA standard.

(D) Intensities of intracellular UCA in neurons from the following brain regions: PFC, M_2, CeA, NAc, DS, and HPC. The digits within the columns represent number of the neurons with intracellular UCA MS signal and number of total measured neurons from 3 mice.

(E) UCA calibration curve constructed by plotting MS intensity against the concentration of the UCA standard. The area marked in gray shows the range of intracellular UCA concentrations in single neurons.

(F) UCA intensity in mouse CSF (N = 6 mice).

Data are represented as mean ± SEM.

See also Figure S1.

measurement of intracellular metabolites at single-neuron level. Recently, we have established a single-cell mass spectrometry (MS) method based on the combination of patch clamp and MS technologies, which can be used to study the metabolic processes of intracellular constituents in single neurons (Zhu et al., 2017). Here, we used this new technology to probe the molecular and metabolic mechanisms in single neurons that regulate UV exposure-induced neurobehavioral changes, such as improved motor learning and recognition memory.

RESULTS

Single-Cell MS Detects UCA in Individual Central Neurons

Using technology that we have recently developed by integrating induced-nanoelectrospray (InESI)/high-resolution-MS with an electrophysiological patch-clamp recording platform, we have detected thousands of possible chemical constituents in single neurons, and more than 50 have been identified in our recent report (Zhu et al., 2017). Beyond the detection of various regular metabolites, such as amino acids, saccharides, lipids, and neurotransmitters, most striking was the discovery of UCA in single hippocampal (HPC) neurons of mice (Figures 1A and 1B), because this small molecule has not previously been reported in the brain. Furthermore, its chemical structure was confirmed by performing tandem MS (MS/MS) on single neurons from the HPC (Figures 1C and S1A). UCA was detected in all examined neurons from six brain regions (Figures 1D and S1B) including the prefrontal cortex (PFC), secondary motor cortex (M_2), central nucleus of the amygdala (CeA), nucleus accumbens (NAc), dorsal striatum (DS), and HPC, suggesting a wide distribution of UCA in the brain. The concentrations of UCA in single neurons

ranged from 55 to 95 μM according to the calibration curve obtained using a UCA standard (Figure 1E). In addition, UCA was present in the cerebrospinal fluid (CSF) (Figure 1F).

UV Exposure Elevates UCA Level in the Brain

Previous reports suggest that UV exposure changes UCA levels in the peripheral skin, blood, and urine (Baden and Pathak, 1967; Kammeyer et al., 1997; Ruegemer et al., 2002). To assess whether UV exposure also alters UCA levels in the brain, we developed a UV-exposure mouse model based on results from previous studies (Fell et al., 2014). Briefly, mice were dorsally shaved and were administered a low dose of 7 μW /cm^2 UVB for 2 hr (Figure 2A), which is equivalent to 30 min of sunlight exposure (D'Orazio et al., 2006; Fell et al., 2014). A significant increase in serum UCA levels was observed after UVB exposure, and this elevation lasted for at least 240 min (Figures 2B, S2A, and S2B). Additionally, UCA levels in the CSF also increased by ~2-fold after 120 min of UVB exposure (Figures 2C and S2C). Moreover, single-cell MS revealed that the intracellular levels of UCA were markedly elevated in single neurons from most brain regions including PFC, M_2, HPC, and DS of mice after 2-hr exposure to UVB light (Figures 2D and 2E). This effect of UVB is reversible because the UVB exposure-induced increase in intracellular level of UCA dropped to near zero when measured at 24 hr after UVB exposure (Figures S2D and S2E).

One possible reason for the increase in brain UCA level after UVB exposure is the entry of elevated UCA in the blood into the brain. To test this idea, we then intravenously (i.v.) injected UCA, which triggered a significant increase in serum UCA levels in a dose-dependent manner (Figure S2F). The UCA dose (i.v., 20 mg/kg) that caused a similar amplitude of increase in blood UCA was selected and used in the later experiments to mimic the UVB-induced elevation of circulating UCA. The i.v. UCA indeed remarkably increased the level of UCA in the CSF of mice (Figures 2F and S2G). Moreover, a significant increase in serum (Figure S2H), CSF (Figures 2G and S2I), and HPC intracellular (Figures 2H and S2J) $^{13}C_3$-UCA was observed after the i.v. administration of 1,2,3-$^{13}C_3$-UCA, thus providing direct evidence that UCA is able to cross the BBB and then enter neurons. Meanwhile, consistent with UVB exposure, i.v. administration of UCA also increased the intracellular UCA level in the same brain regions including PFC, M_2, HPC, and DS (Figures 2I, S2K–S2M, and S2O). Surprisingly, neither UVB exposure nor i.v. UCA affected intracellular level of UCA in NAc neurons (Figures 2E, 2I, and S2N), possibly due to a much lower permeability of BBB for certain small molecules in NAc compared to other brain regions (Figures S2P–S2U). Overall, these findings suggest that the circulating UCA may be capable of crossing the BBB and entering neurons in most brain areas.

Histidine-UCA-Glutamate: A Novel Glutamate Biosynthetic Pathway in Neurons

UCA has been reported to exist only in the peripheral system, such as skin, liver, blood, and urine (Baden and Pathak, 1967; Cook, 2001; Kammeyer et al., 1997; Ruegemer et al., 2002). In mammal liver and other peripheral tissues, UCA is an intermediate in the conversion of histidine (HIS) to glutamate (GLU) (Figure 3A) (Brown and Kies, 1959; Cook, 2001; Merritt et al., 1962). Interestingly, our single-cell MS analysis detected not only HIS, UCA, and GLU but also two other intermediates involved in the liver HIS-UCA-GLU metabolic pathway, specifically 4-imidazolone-5-propionic acid (IPPA) and formiminoglutamic acid (FMGA), in single HPC neurons (Figures 3B–3D and S3A–S3D).

To verify the existence of HIS-UCA-GLU metabolic pathway throughout the brain, using single-cell MS technology, we collected and analyzed the intracellular samples from >300 neurons randomly selected in 15 brain regions in the sagittal mouse brain slices pre-incubated with HIS or saline. HIS incubation significantly induced a 1- to 2-fold increase in the intracellular level of UCA, IPPA, FMGA, and GLU in all brain regions, suggesting a wide distribution of HIS-GLU metabolic pathway throughout the brain (Figures S3E–S3H). It is likely that this GLU biosynthetic pathway may exist in specific cell types in the brain because the amplitudes of increase in these HIS metabolites varied in distinct neurons, even from the same brain region (Figures S3E–S3H).

Stable isotopic ^{13}C-labeling is one of the most common methods used to identify *in vivo* chemical metabolic pathways (Zamboni et al., 2009). Therefore, we next incubated PFC neurons in brain slices with ^{13}C-labeled HIS (1-^{13}C-HIS) for 1 hr, extracted intracellular constituents, and analyzed them using singe-cell MS. We observed significantly higher ^{13}C-HIS/HIS, ^{13}C-UCA/UCA, ^{13}C-GLU/GLU, and ^{13}C-IPPA/IPPA ratios in neurons pre-incubated with ^{13}C-HIS compared with those in untreated neurons (Figures 3E and S3I–S3L), thus providing direct evidence of the conversion of HIS to UCA and GLU in single neurons.

Additionally, western blotting analysis suggested that key enzymes involved in the liver HIS-UCA-GLU pathway, including histidase, urocanase, and imidazolonepropionase (IPPAnase), are also present in many brain regions, including the PFC, motor cortex (MC), NAc, DS, CeA, HPC, superior colliculus (SC), hypothalamus (HT), cerebellum (CB), and brain stem (BS) (Figures 3F, 3G, and S3M–S3P). The expression of these key enzymes was also demonstrated by immunohistochemistry and *in situ* hybridization (Figures S3Q–S3T). Additionally, these enzymes were also detected in synaptosomes isolated from the mouse brain, suggesting an existence of this metabolic pathway in the neuronal synaptic terminals (Figure S3U).

Next, dipeptide glycyl-glycine (GG) as the urocanase inhibitor (Hunter and Hug, 1989) was applied to test the physiological roles of urocanase in neurons (Figures S3V–S3KK). Incubation with either HIS or UCA dramatically increased the concentration of GLU in neurons, and this effect was abolished by preincubation with GG (Figures 3H, 3I, and S3LL–S3PP). Furthermore, the i.v. injection of $^{13}C_3$-UCA significantly increased the $^{13}C/^{12}C$ ratio of $^{13}C_3$-UCA, $^{13}C_3$-IPPA, $^{13}C_3$-FMGA, and $^{13}C_3$-GLU in single neurons of HPC (Figure S2J), suggesting that the UCA-GLU metabolic pathway functions *in vivo* as well.

UV Exposure Promotes GLU Biosynthesis in the Brain

Single-cell MS revealed that intracellular levels of metabolites involved in UCA-GLU pathway, including UCA, IPPA, FMGA, and GLU, were all markedly increased in single neurons of mice after exposure to UVB light (Figures S4A-S4D; Table S3).

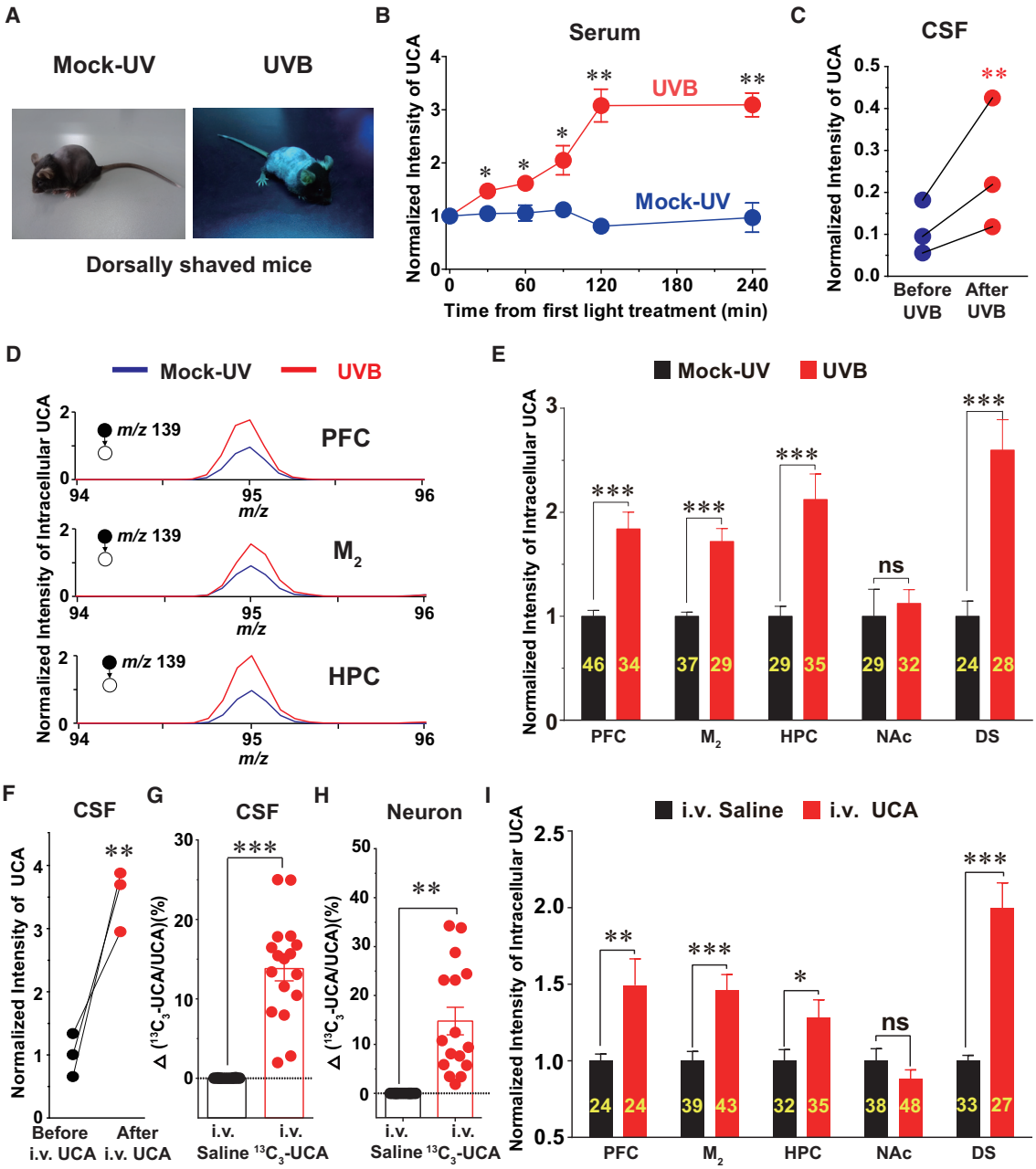

Figure 2. Effects of UVB Exposure on UCA Levels in the Serum, CSF, and Single Neurons

(A) Representative mice subjected to mock-UV or UVB exposure.

(B) Time course of UCA levels in mouse serum during 4 hr of mock-UV (blue line, N = 3 mice) or UVB exposure (red line, N = 4 mice). Data were normalized to their respective controls (0 min, mock-UV).

(C) UCA levels in mouse CSF before (blue dots, N = 3 mice) and after (red dots, N = 3 mice) 2 hr of mock-UV or UVB exposure.

(D and E) Representative MS/MS spectra (D) and normalized intensities (E) of intracellular UCA in single neurons of the PFC, M_2, HPC, NAc, and DS in mice exposed to mock-UV or UVB. All data were normalized to their respective controls (mock-UV groups).

(F) The normalized intensities of UCA in the CSF before and after i.v. injection of UCA (20 mg/kg, 30 min).

(G and H) The normalized $^{13}C_3$-UCA/UCA ratio in the mouse CSF (G) and single HPC neurons (H) after i.v. injection of saline or $^{13}C_3$-UCA (20 mg/kg, 30 min).

(I) The normalized intensities of intracellular UCA in single neurons from the PFC, M_2, HPC, NAc, and DS of mice after i.v. injection of UCA (20 mg/kg, 30 min) or saline. All data were normalized to their respective controls (i.v. saline group).

All digits within the columns represent numbers of total neurons measured from 3 mice. Data are represented as mean ± SEM. *$p < 0.05$, **$p < 0.01$, ***$p < 0.001$, ns, not significant ($p > 0.05$) based on unpaired t test.

See also Figure S2.

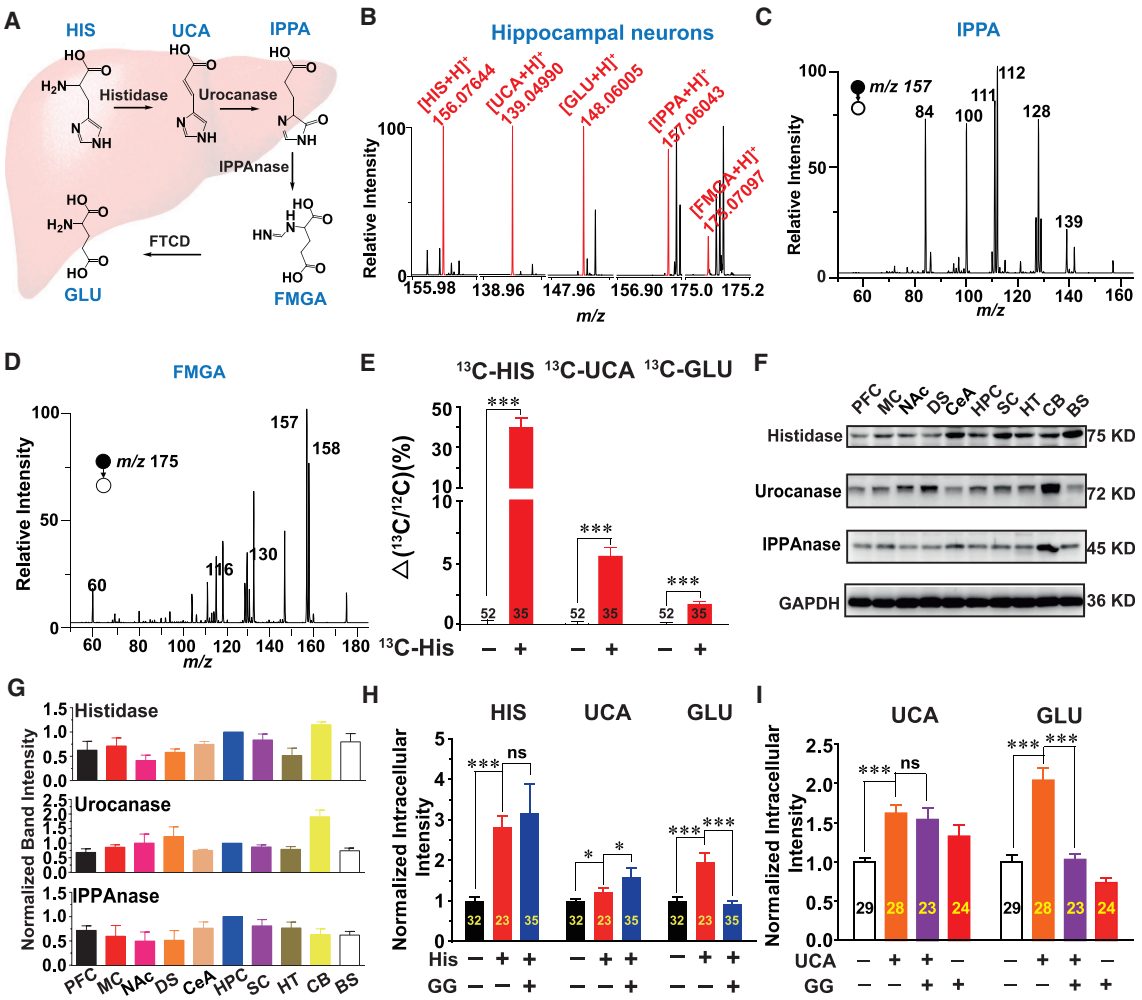

Figure 3. Identification of the HIS-UCA-GLU Metabolic Pathway in Neurons

(A) Metabolic pathway from HIS to GLU in the liver. FTCD means formimidoyltransferase-cyclodeaminzase.

(B) Single-cell MS shows the coexistence of HIS, UCA, IPPA, FMGA, and GLU in single HPC neurons.

(C and D) Confirmation of IPPA (C) and FMGA (D) structure using tandem MS.

(E) Identification of the HIS-UCA-GLU metabolic pathway via ^{13}C-labeling in single neurons. ^{13}C-HIS/HIS, ^{13}C-UCA/UCA, and ^{13}C-GLU/GLU ratios in single neurons from the HPC slices with or without ^{13}C-HIS (3 mg/mL, 1 hr) preincubation.

(F and G) Western blot (F) and normalized band intensity (G) of histidase, urocanase and IPPAnase in several mouse brain regions including PFC, MC, NAc, DS, CeA, HPC, SC, HT, CB, and BS. Data were normalized to values of HPC.

(H) Normalized intensities of intracellular HIS, UCA, and GLU in single HPC neurons with or without preincubation of HIS (0.2 mg/mL) or GG (0.13 mg/mL).

(I) Normalized intensities of intracellular UCA and GLU in single HPC neurons with or without preincubation of UCA (0.7 mg/mL) or GG (0.13 mg/mL). All data were normalized to their respective controls (neurons pre-incubated with vehicles).

All digits within the columns represent numbers of total neurons measured from 3 mice. Data are represented as mean ± SEM. *$p < 0.05$, ***$p < 0.001$ ns, not significant ($p > 0.05$) based on unpaired t test.

See also Figure S3.

The urocanase inhibitor GG blocked the UV-induced increase in GLU (Figures 4A and 4B) but not UCA (Figure S4E) in these neurons, thus suggesting that UVB exposure-induced GLU elevation is primarily due to the activation of the UCA-GLU metabolic pathway in brain. This hypothesis was further confirmed by evidence showing that the knockdown of urocanase expression (Figure S4F) using lentiviral short hairpin RNAs (shRNAs) also considerably inhibited UVB exposure-induced increases in GLU (Figures 4C and 4D) but not UCA (Figure S4G) in HPC neurons. Furthermore, intra-HPC injection of AAV-shRNA against IPPAnase attenuated the UVB exposure-induced increase in intracellular levels of FMGA, but not UCA and IPPA, while intra-HPC injection of AAV-shRNA against FTCD only blocked the UVB exposure-induced increase in intracellular levels of GLU, but not UCA, IPPA, and FMGA (Figures S4H and S4I). Interestingly, both intracerebroventricular (i.c.v.) injection of GG alone and intra-HPC injection of urocanase, IPPAnase, or FTCD shRNA alone significantly increased the intracellular level of

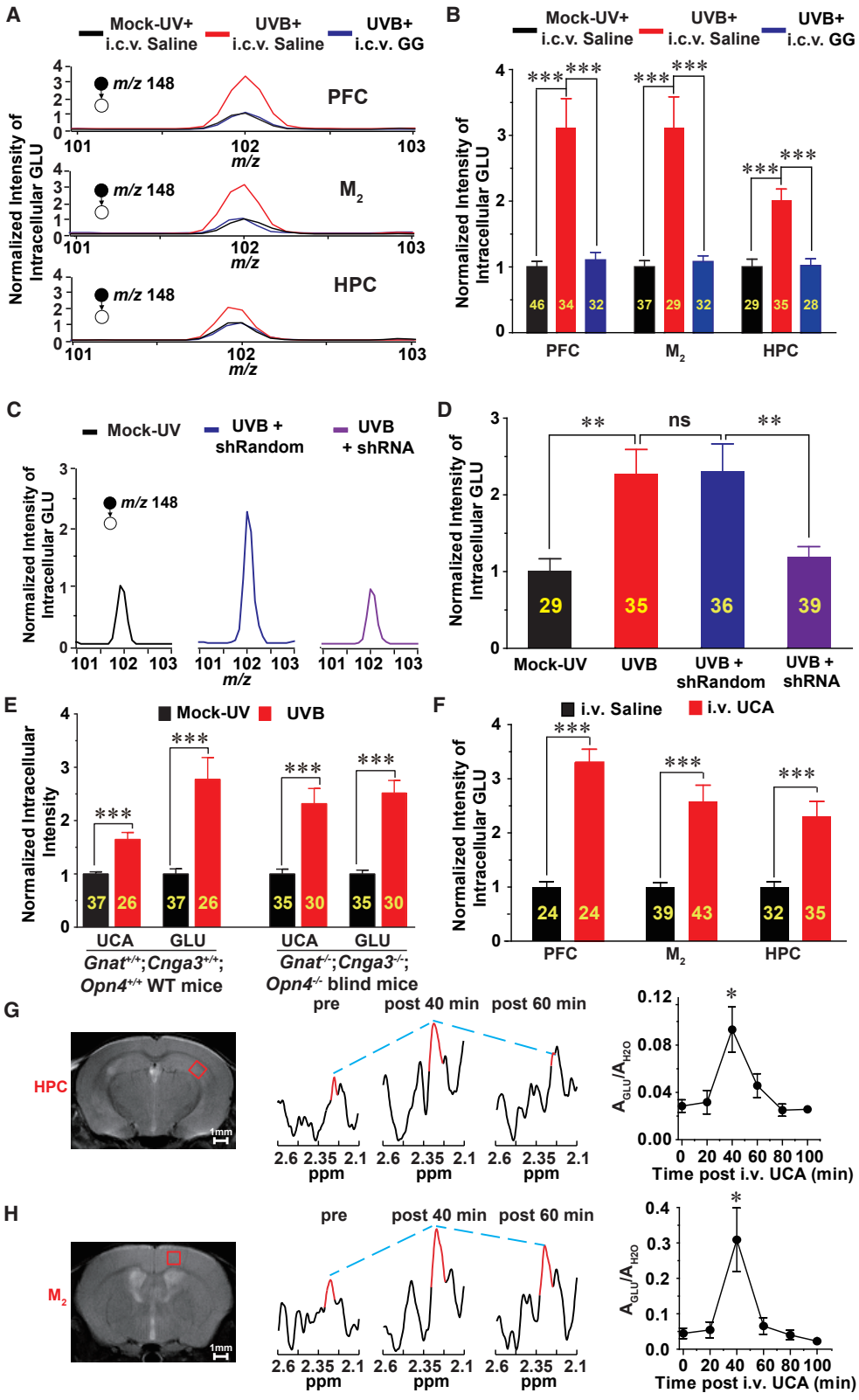

(legend on next page)

UCA and decreased the intracellular level of GLU, suggesting a possible contribution of the endogenous UCA-GLU metabolic pathway to glutamate pools in neurons (Figures S4J–S4M).

To exclude the possibility that UVB light might cause an elevation in brain UCA and GLU through the visual system of mice, we used triple knockout (*Gnat*$^{-/-}$;*Cnga3*$^{-/-}$;*Opn4*$^{-/-}$) mice that lack functional photoreceptors in their retinas and are completely blind (Xue et al., 2011). UVB exposure still markedly increased UCA and GLU levels in single neurons of the HPC in these blind mice (Figures 4E and S4N–S4Q), thus suggesting a mechanism independent of the visual system.

We again i.v.-injected UCA to mimic the UVB-induced increase in blood UCA. Single-cell MS revealed a significant increase in the concentration of GLU in single neurons from various brain regions, including the PFC, M_2, HPC, and DS but not the NAc (Figures 4F and S4R–S4U).

In vivo ^{1}H magnetic resonance spectroscopy (MRS) was applied to detect GLU signals according to the primary resonance peaks that exhibited a chemical shift around 2.3 ppm, which represent the GLU concentration in the brain (Zielman et al., 2017). Experiments were carried out to determine whether the systemic administration of UCA affects GLU levels in the brain *in vivo* (Figure S4V). Our MRS data from mice at 9.4T consistently showed a significant elevation of GLU signals in both the HPC (Figure 4G) and M_2 (Figure 4H) at 40 min after i.v. UCA injection.

Glutamatergic Synaptic Transmission Is Enhanced following UVB Exposure

In addition to participating in protein synthesis and cellular energy metabolism (Nedergaard et al., 2002), GLU plays indispensable roles as an excitatory neurotransmitter in the vertebrate nervous system (Meldrum, 2000; van den Pol et al., 1990). It is unclear whether UVB exposure-induced increases in GLU in neurons affect glutamatergic synaptic transmission. Using electrophysiological recording of brain slices, we next examined GLU release by neuronal projections from the HPC CA3 area to the CA1 area as an example, because this pathway is one of the two main glutamatergic inputs received by CA1 neurons (Sun et al., 2014; Takács et al., 2012). First, the pAAV-mCamKIIα-hChR2(H134R)-EGFP virus was injected into CA3 to express channelrhodopsin 2 (ChR2) along the GLU$^{CA3\rightarrow CA1}$ neuronal projections (Figures 5A and 5B). Then, CA1 pyramidal neurons were patched, and only those neurons responding to optical stimulation with blue light (473 nm) were selected for subsequent tests (Figure 5C). The miniature excitatory postsynaptic currents (mEPSCs), which result from the spontaneous release of GLU quanta from individual vesicles, were recorded in the hippocampal slices after the mice were exposed to mock-UV or UVB (Figure 5D). UVB exposure significantly increased the amplitude (Figure 5E) but not the frequency of mEPSCs (Figure S5A), thus suggesting a possible increase in GLU levels in the neuronal terminals. Moreover, this effect was attenuated by the i.c.v. administration of GG (Figures 5E and S5A) or intra-HPC CA3 injection of AAV-shRNA against urocanase before UVB exposure (Figures 5F and S5B).

The increase in amplitude of mEPSCs may be attributable to more GLU content packaging per quanta (i.e., per presynaptic vesicle), in agreement with our findings that UVB exposure increases intracellular GLU levels in HPC neurons, as mentioned above. To confirm this possibility, we used a method combining optogenetics and multiple-probability fluctuation analysis (MPFA), which facilitates the input-specific quantification of quantal parameters of glutamatergic synaptic transmission (Mitchell and Silver, 2000; Suska et al., 2013). To stimulate GLU$^{CA3\rightarrow CA1}$ presynaptic terminals, we optically applied a five-pulse train (at 20 Hz), which was used to set excitatory synapses to five repetitive and consistent release states for the MPFA (Figure 5G). Data from individual cells typically fit a symmetrical parabola curve (Figure 5H), in agreement with a binomial model of synaptic transmission (Mitchell and Silver, 2000; Suska et al., 2013). Quantal size (Q), representing the GLU concentration in single presynaptic vesicles from GLU$^{CA3\rightarrow CA1}$ neuron-projecting terminals, significantly increased after UVB exposure (Figure 5I). However, other possible factors affecting glutamatergic transmission, such as the number of synapses (N) and the release probability (Pr), were not altered by UVB exposure (Figures S5C and S5D). Furthermore, the UVB exposure-induced increase in Q value was also diminished by intra-HPC CA3 injection of AAV-shRNA

Figure 4. Effects of UVB Exposure and i.v. UCA Administration on GLU Levels in the Brain

(A and B) Representative MS/MS spectra (A) and normalized intensities (B) of intracellular GLU in single neurons of the PFC, M_2, and HPC in mice with or without mock-UV treatment, UVB exposure, and intracerebroventricular (i.c.v.) infusion of GG (2.6 μg, 1 μL). Data were normalized to their respective controls (mock-UV groups without i.c.v. injection of GG).

(C and D) Representative MS/MS spectra (C) and normalized intensity (D) of intracellular GLU showing the effects of intra-HPC injection of lentiviral shRNA (0.5 μ/side, 10^9 TU/mL) against urocanase (shRNA) or random control shRNA (shRandom, 0.5 μL/side, 10^9 TU/mL) on the UVB-induced elevation of intracellular GLU levels in single HPC neurons.

(E) Normalized intensities of intracellular UCA and GLU in single HPC neurons of *Gnat*$^{-/-}$;*Cnga3*$^{-/-}$;*Opn4*$^{-/-}$ blind mice and *Gnat*$^{+/+}$;*Cnga3*$^{+/+}$;*Opn4*$^{+/+}$ wild-type (WT) mice after mock-UV or UVB exposure. Data were normalized to their respective controls (mock-UV group).

(F) Normalized intensities of intracellular GLU in single neurons from the PFC, M_2 and HPC of mice following the i.v. injection of UCA (20 mg/kg, 30 min) or saline. Data were normalized to their respective controls (i.v. saline group).

(G and H) HPC CA3 (G, left) and M_2 (H, left) are outlined (red squares) on T_2-weighted images of mouse brain. ^{1}H MRS of GLU in the HPC (G, middle) and M_2 (H, middle) were measured using high field (9.4T) magnetic resonance imaging (MRI) after the i.v. administration of UCA (20 mg/kg). Quantification of GLU signals in the HPC (G, right) and M_2 (H, right) every 20 min (from 0 to 100 min) after the i.v. injection of UCA (20 mg/kg). A_{GLU}/A_{H2O} means the ratio of GLU signal integral of peak area over H_2O signal.

All digits within the columns represent numbers of total neurons measured from 3 mice. Data are represented as mean ± SEM. *$p < 0.05$, **$p < 0.01$, ***$p < 0.001$, ns, not significant ($p > 0.05$) based on unpaired t test.

See also Figure S4 and Table S3.

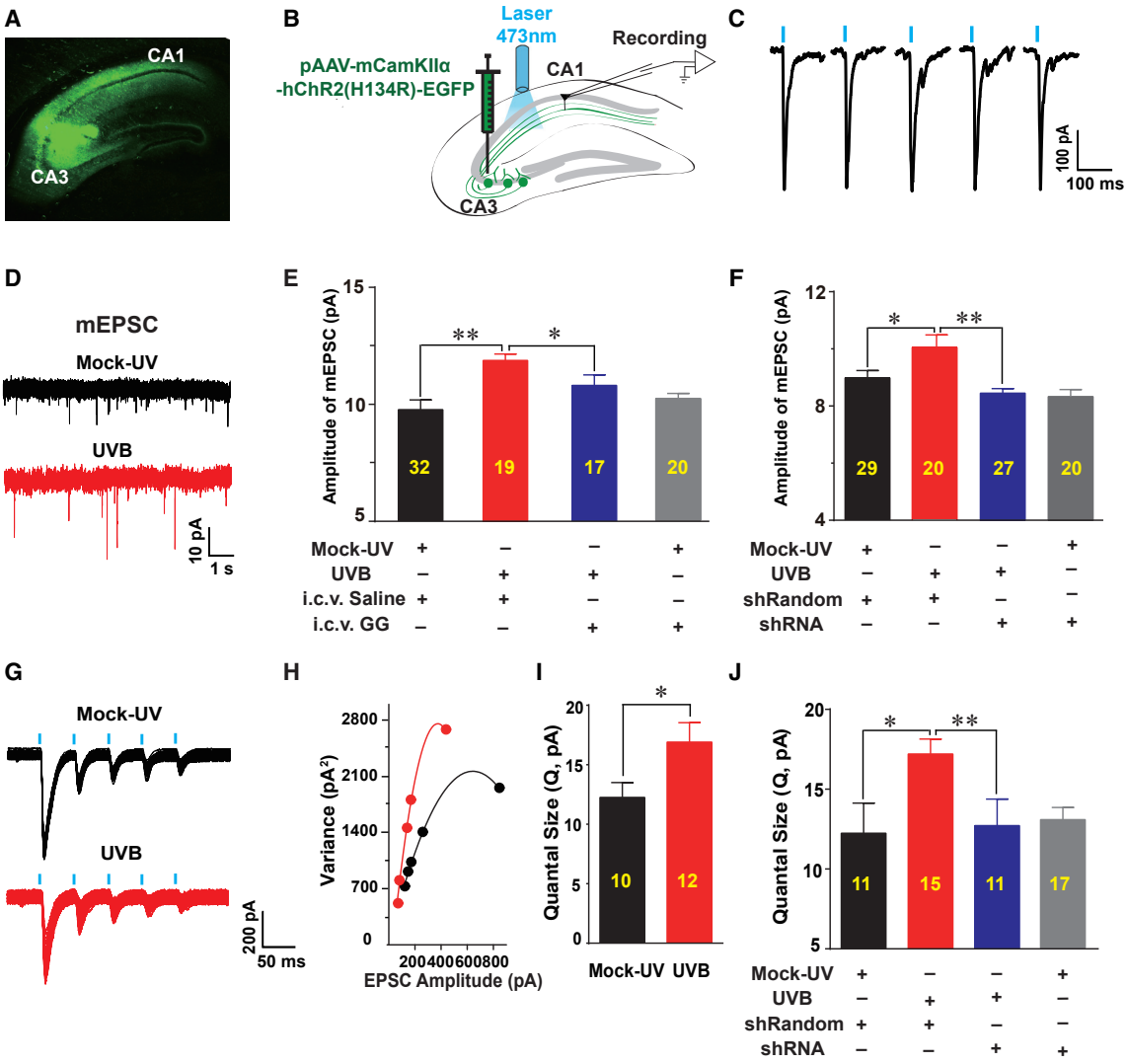

Figure 5. Effects of UVB Exposure on Glutamatergic Synaptic Transmission from HPC CA3 to CA1

(A) Representative image showing the viral expression of pAAV-mCamKIIα-hChR2(H134R)-EGFP along the neuronal projections from HPC CA3 to CA1.

(B) Schematic image showing the electrophysiological recording of CA1 pyramidal neurons after the optical stimulation of $GLU^{CA3\rightarrow CA1}$ projecting fibers.

(C) Trace records of blue light (473 nm, 5 ms) evoked EPSC in CA1 pyramidal neurons. Neurons responding to optical stimulation were selected for subsequent recordings.

(D) Trace records of mEPSCs of CA1 neurons from mice with mock-UV or UVB exposure.

(E) Average amplitudes of mEPSCs of CA1 neurons from mice with or without mock-UV, UVB exposure, and i.c.v. injection of GG (2.6 μg, 1 μL).

(F) Average amplitudes of mEPSCs of CA1 neurons from mice with or without mock-UV, UVB exposure, and intra-HPC injection of AAV-shRNA (0.5 μL/side, 1.3×10^{12} vg/mL) against urocanase or random control shRNA (shRandom, 0.5 μL/side, 1.6×10^{12} vg/mL).

(G) EPSCs were triggered by the optical stimulation of $GLU^{CA3\rightarrow CA1}$ neuronal fibers. Example traces of 100 overlapping synaptic responses from mice exposed to mock-UV or UVB.

(H) MPFA of the example recordings in (G).

(I) The quantal parameters Q were derived from the parabolic fit of the variance-mean analysis.

(J) Effects of intra-HPC injection of AAV-shRNA (0.5 μl/side, 1.3×10^{12} vg/mL) against urocanase on UVB exposure-induced increase in the quantal parameters Q.

All digits within the columns represent numbers of total neurons measured from at least 3 mice. Data are represented as mean ± SEM. *$p < 0.05$, **$p < 0.01$ based on unpaired t test.

See also Figure S5.

against urocanase (Figure 5J). Except for vesicular glutamate content, the other factor affecting quantal size is the alteration of synaptic AMPA receptors. This possibility can be excluded because the ratio of AMPA to NMDA receptor components of evoked excitatory postsynaptic currents (eEPSCs) was not influenced by UVB exposure (Figure S5E).

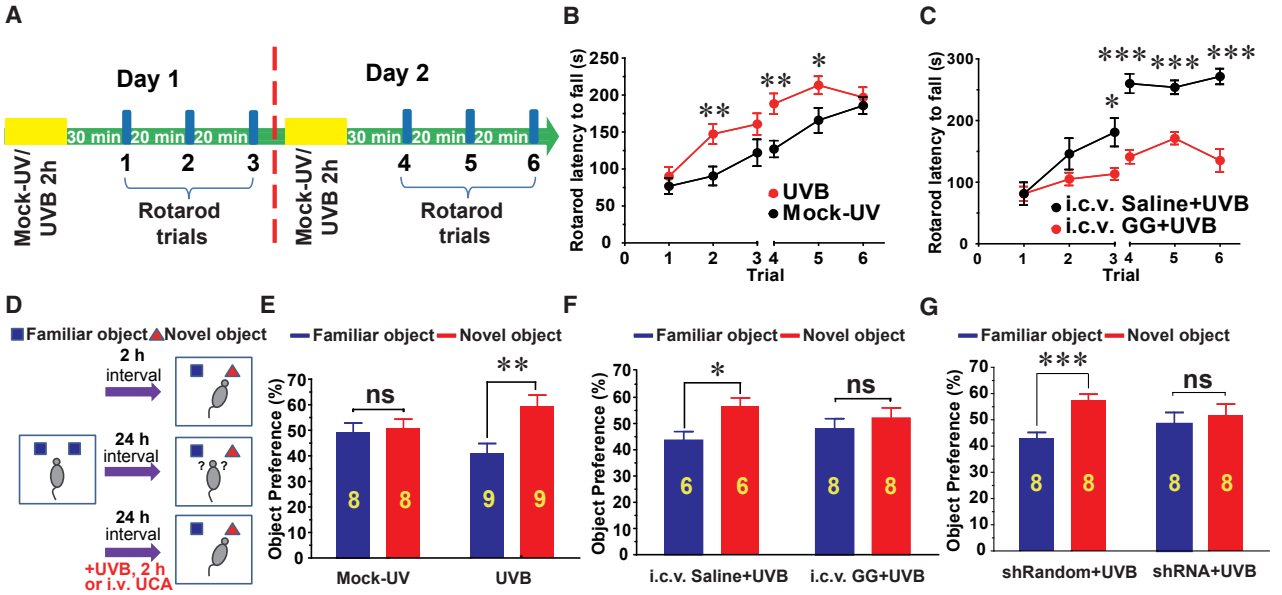

Figure 6. Effects of UVB Exposure on Motor Learning and Object Recognition Memory

(A) Experimental design of the rotarod test.

(B) Latency to fall on the accelerating rotarod for each trial on days 1 and 2 in mice after mock-UV or UVB exposure.

(C) Time spent on the rotarod by mice after the i.c.v. administration of GG (13.2 μg, 1 μL, red dots, N = 6 mice) or saline as a control (black dots, N = 9 mice) followed by UVB exposure.

(D) Diagram of novel object recognition memory tasks.

(E) The preference of mice for familiar and novel objects during a 3-min test at 24 hr after familiarization. Mice were exposed to mock-UV or UVB for 2 hr before the test.

(F) The object preference of mice after i.c.v. injection of GG (13.2 μg, 1 μL) or saline and subsequent UVB exposure.

(G) The object preference of mice after intra-HPC CA3 injection of urocanase shRNA (0.5 μL/side, 10^9 TU/mL) or shRandom (0.5 μL/side, 10^9 TU/mL) and subsequent UVB exposure.

All digits within the columns represent numbers of mice in each group. Data are represented as mean ± SEM. *$p < 0.05$, **$p < 0.01$, ***$p < 0.001$, ns, not significant ($p > 0.05$) based on unpaired t test;

See also Figure S6.

Evidence has emerged suggesting that the projecting neurons from MC to DS are also glutamatergic (Hintiryan et al., 2016; Kreitzer and Malenka, 2008; Rothwell et al., 2015; Yin et al., 2009). Therefore, we next measured GLU release by neuronal projections from M_2 to DS because intracellular GLU levels in M_2 also increased after UVB exposure (Figure 4B). Anterograde tracing with pAAV-mCamKIIα-hChR2(H134R)-EGFP indeed verified the glutamatergic pathway from M_2 to DS (Figure S5F). A similar scenario occurred in the $GLU^{M2\rightarrow DS}$ circuit, where UVB exposure significantly increased the mEPSC amplitude and presynaptic quantal size of GLU (Figures S5F–S5P).

UVB Exposure Improves Motor Learning and Recognition Memory via the UCA-GLU Metabolic Pathway in the Brain

Emerging evidence has suggested that the glutamatergic circuit from the MC to the DS is involved in motor learning (Rothwell et al., 2015; Yin et al., 2009). Therefore, we asked whether UVB exposure affects motor learning ability by initiating the UCA-GLU metabolic pathway in M_2 neurons and subsequently activating $GLU^{M2\rightarrow DS}$ circuits. Mice received 50 mJ/cm^2 UVB exposure before 3 trials with typical accelerating rotarod training each day for 2 days (Figure 6A). The motor skill learning of mice in the accelerating rotarod task was dramatically improved after UVB exposure (Figure 6B). This effect was markedly inhibited by the i.c.v. administration of GG 15 min before UVB exposure (Figure 6C). To mimic the UVB-induced increase in circulating UCA, we intravenously injected UCA and observed that the rotarod skill learning ability of the mice was also significantly enhanced (Figure S6A). Additionally, this effect was blocked by the i.c.v. injection of GG (Figure S6B).

Additionally, a large body of evidence suggests a role of $GLU^{CA3\rightarrow CA1}$ neurons in long-term recognition memory (Brun et al., 2002; Clarke et al., 2010). Thus, we next carried out a novel object recognition test to determine whether UVB exposure affects the recognition memory of mice and whether the intracellular UCA-GLU metabolic pathway in HPC CA3 neurons is involved. Mice were exposed to two identical objects placed at an equal distance (Figure 6D). The time spent exploring each object was recorded, and the object preference percentage demonstrated no distinction between both objects on the left and right sides (Figure S6C). The next day, the mice were allowed to explore the open field in the presence of a familiar object and a novel object to test recognition memory. Long-term (24 hr), but not short-term (2 hr), recognition memory of mice was significantly improved by the UVB exposure (Figure 6E) as well as the i.v. administration of

UCA (Figures S6D and S6E). Interestingly, despite of distinct sensitivities of the skin of different genders to UV light, there was little difference between male and female mice in terms of UVB exposure-induced changes in brain UCA-GLU metabolic pathway, rotarod learning, and object recognition memory (Figures S6–S6H). The UVB exposure-induced improvement of recognition memory was markedly diminished by either i.c.v. injection of a urocanase inhibitor (Figures 6F, S6I, and S6J) or knockdown of urocanase expression in the HPC CA3 regions by using a lentiviral shRNA against urocanase (Figures 6G, S6K, and S6L).

DISCUSSION

This study provides the first evidence of a novel GLU biosynthetic pathway in neurons, as detected with our recently developed single-cell InESI/MS technology (Zhu et al., 2017). Although the HIS-UCA-GLU pathway in the liver has been previously described (Brown and Kies, 1959; Cook, 2001; Merritt et al., 1962), it is unclear whether this pathway exists in the CNS. All metabolites and enzymes related to the liver HIS-UCA-GLU pathway were also present in single neurons in various brain regions. A detailed pathway was further confirmed by direct evidence showing that incubation with ^{13}C-HIS and i.v. injection of ^{13}C-UCA both resulted in a significant increase in ^{13}C-UCA and ^{13}C-GLU in single neurons. These discoveries expand knowledge of other biosynthetic GLU pathway in neurons beyond the quintessential pathways, such as the tricarboxylic acid cycle originating with glucose and the GLU-glutamine cycle between neurons and astrocytes (Bélanger et al., 2011). The presence of HIS-UCA-GLU pathway in the CNS is supported by the clinical findings showing that histidinemia and urocanic aciduria, which are autosomal recessive metabolic disorders due to histidase and urocanase deficiency respectively, are both associated with multiple central developmental symptoms, including learning difficulties, speech or language disturbances, subnormal intelligence, and mental retardation (Davies and Robinson, 1963; Espinós et al., 2009; Kalafatic et al., 1980; Lott et al., 1970; Raisová and Hyánek, 1986), presumably because of lower GLU synthesis in neurons during brain development, based upon our findings.

This study indicates that the single-cell MS technology is a valuable tool to study novel metabolic pathways in the brain at the single-cell level. The use of single-cell MS to study cell metabolism is more advantageous than conventional methods using tissue homogenates or cell populations, which are limited to the measurement of average values. For example, UCA has previously been identified in the peripheral system, including the blood, skin, liver, and urine (Baden and Pathak, 1967; Cook, 2001; Kammeyer et al., 1997; Ruegemer et al., 2002). However, it has not previously been detected in the CNS. Conventional chemical analysis using brain tissue homogenates may result in several drawbacks, such as the over-dilution of constituents at low concentrations, cellular diversity and complexity, and possible decomposition during tedious sample pretreatment and chromatographic separation (Altschuler and Wu, 2010; Zenobi, 2013), all of which greatly affect the precise measurement of target compounds.

Although overexposure to UV radiation may cause several adverse health effects, moderate UV exposure greatly benefits physical and mental health at multiple levels. Moderate UV-light exposure affects behaviors related to the CNS, such as emotion, learning, and memory (Beecher et al., 2016; Benedetti et al., 2001; Cunningham, 1979; Dominiak et al., 2015; Fell et al., 2014; Keller et al., 2005; Parrott and Sabini, 1990), although it is far from clear what mechanism mediates this phenomenon. We demonstrate that UV exposure triggers elevation of blood UCA, which in turn crosses the BBB and enters neurons to participate in the biosynthesis of GLU. The increase in neuronal GLU synthesis may result in more GLU packaging into synaptic vesicles and more GLU release from nerve terminals, thus strengthening glutamatergic neural circuits such as GLU$^{M2\rightarrow DS}$ or GLU$^{CA3\rightarrow CA1}$projections and related behaviors such as motor learning and recognition memory. Our results may suggest a universal mechanism for UV exposure-induced neurobehavioral changes related to the CNS: certain chemical substances generated in the blood by UV exposure enter the brain through the BBB and then alter neuronal excitability. Additional strong evidence supporting this hypothesis consists of a recent finding that UV exposure elevates circulating β-endorphin, which acts on the CNS and results in opioid receptor-mediated addiction to UV light (Fell et al., 2014). Because GLU plays multiple roles in the CNS, including protein biosynthesis at the amino acid level (Nedergaard et al., 2002), disposal of excess or waste nitrogen (Melo-Oliveira et al., 1996), and signal transduction between neurons as the most abundant excitatory neurotransmitter (Meldrum, 2000; van den Pol et al., 1990), the UV-activated intracellular UCA-GLU metabolic pathway in neurons is likely to be involved in sunbathing-related neurological conditions in addition to learning and memory, such as mood improvement, addiction, cognition, and brain development.

STAR★METHODS

Detailed methods are provided in the online version of this paper and include the following:

- KEY RESOURCES TABLE
- CONTACT FOR REAGENT AND RESOURCE SHARING
- EXPERIMENTAL MODEL AND SUBJECT DETAILS
  - Mice
  - Cell Culture
- METHOD DETAILS
  - UVB Irradiation
  - Mouse Serum and Cerebrospinal Fluid (CSF) Preparation
  - Brain Slice Preparation
  - Single-Neuron MS
  - ^{13}C-Isotope Tracing Experiments
  - Calibration Curves of UCA
  - Lentivirus Production and Transduction
  - RNA Interference
  - Synaptosomal Preparation
  - Western Blotting
  - Brain Tissue Preparation and Immunohistochemistry
  - Fluorescent *in Situ* Hybridization (FISH) Experiment
  - Magnetic Resonance Imaging Experiments
  - Electrophysiological Recording

SUPPLEMENTAL INFORMATION

Supplemental Information includes six figures and three tables and can be found with this article online at https://doi.org/10.1016/j.cell.2018.04.014.

ACKNOWLEDGMENTS

The authors thank Dr. Yang Pan (National Synchrotron Radiation Laboratory, University of Science and Technology of China) for instrumentation supports. The authors thank Dr. Li Zhang (National Institute on Alcohol Abuse and Alcoholism, National Institutes of Health, USA), Dr. Yong Shen (University of Science and Technology of China), and the anonymous reviewers for valuable comments and suggestions to improve the quality of the paper. We acknowledge support from National Key R&D Program of China (2016YFC1300500-2 to W.X. and 2016YFA0201300-2 to G.H.), National Natural Science Foundation of China (31471014, 91432103, and 91649121 to W.X., 21775143 and 21475121 to G.H., and 81701068 to H.Z.), the Strategic Priority Research Program of the Chinese Academy of Sciences (XDB02010000 to W.X.), the Fundamental Research Funds for the Central Universities (W.X. and G.H.), the Major/Innovative Program of Development Foundation of Hefei Center for Physical Science and Technology (2017FXZY006 to W.X. and 2017FXCX003 to G.H.), and Recruitment Program of Global Experts (W.X. and G.H.).

AUTHOR CONTRIBUTIONS

W.X. and G.H. designed research and supervised the project. H.Z., N.W., and Q.C. conducted electrophysiological recordings and single-cell MS. L.Y. conducted western blot experiments. W.G. and S.F. conducted immunohistochemistry. S.L. and J.L. conducted *in situ* hybridization. Y.H., F.D., Q.Z., Y.G., X.Z., and Y.X. conducted animal behavioral tests. R.Z. and X.S. produced the lentiviral shRNA. T.X. generated the triple knockout blind mice. J.Q. and K.Z. conducted magnetic resonance imaging experiments. H.Z., N.W., W.X., and G.H. analyzed data. W.X., H.Z., and G.H. wrote the manuscript.

DECLARATION OF INTERESTS

The authors declare no competing interests.

Received: August 17, 2017
Revised: February 21, 2018
Accepted: April 12, 2018
Published: May 17, 2018

REFERENCES

Ada, S., Seçkin, D., Budakoğlu, I., and Ozdemir, F.N. (2005). Treatment of uremic pruritus with narrowband ultraviolet B phototherapy: an open pilot study. J. Am. Acad. Dermatol. *53*, 149–151.

Altschuler, S.J., and Wu, L.F. (2010). Cellular heterogeneity: do differences make a difference? Cell *141*, 559–563.

Archier, E., Devaux, S., Castela, E., Gallini, A., Aubin, F., Le Maître, M., Aractingi, S., Bachelez, H., Cribier, B., Joly, P., et al. (2012). Carcinogenic risks of psoralen UV-A therapy and narrowband UV-B therapy in chronic plaque psoriasis: a systematic literature review. J. Eur. Acad. Dermatol. Venereol. *26* (*Suppl 3*), 22–31.

Baden, H.P., and Pathak, M.A. (1967). The metabolism and function of urocanic acid in skin. J. Invest. Dermatol. *48*, 11–17.

Barresi, C., Stremnitzer, C., Mlitz, V., Kezic, S., Kammeyer, A., Ghannadan, M., Posa-Markaryan, K., Selden, C., Tschachler, E., and Eckhart, L. (2011). Increased sensitivity of histidinemic mice to UVB radiation suggests a crucial role of endogenous urocanic acid in photoprotection. J. Invest. Dermatol. *131*, 188–194.

Beecher, M.E., Eggett, D., Erekson, D., Rees, L.B., Bingham, J., Klundt, J., Bailey, R.J., Ripplinger, C., Kirchhoefer, J., Gibson, R., et al. (2016). Sunshine on my shoulders: weather, pollution, and emotional distress. J. Affect. Disord. *205*, 234–238.

Bélanger, M., Allaman, I., and Magistretti, P.J. (2011). Brain energy metabolism: focus on astrocyte-neuron metabolic cooperation. Cell Metab. *14*, 724–738.

Benedetti, F., Colombo, C., Barbini, B., Campori, E., and Smeraldi, E. (2001). Morning sunlight reduces length of hospitalization in bipolar depression. J. Affect. Disord. *62*, 221–223.

Bouillon, R. (2017). Comparative analysis of nutritional guidelines for vitamin D. Nat. Rev. Endocrinol. *13*, 466–479.

Brown, D.D., and Kies, M.W. (1959). The mammalian metabolism of L-histidine. II. The enzymatic formation, stabilization, purification, and properties of 4(5)-imidazolone-5(4)-propionic acid, the product of urocanase activity. J. Biol. Chem. *234*, 3188–3191.

Brun, V.H., Otnass, M.K., Molden, S., Steffenach, H.A., Witter, M.P., Moser, M.B., and Moser, E.I. (2002). Place cells and place recognition maintained by direct entorhinal-hippocampal circuitry. Science *296*, 2243–2246.

Clarke, J.R., Cammarota, M., Gruart, A., Izquierdo, I., and Delgado-García, J.M. (2010). Plastic modifications induced by object recognition memory processing. Proc. Natl. Acad. Sci. USA *107*, 2652–2657.

Cook, R.J. (2001). Disruption of histidine catabolism in NEUT2 mice. Arch. Biochem. Biophys. *392*, 226–232.

Cunningham, M.R. (1979). Weather, mood, and helping behavior: quasi experiments with the Sunshine Samaritan. J. Pers. Soc. Psychol. *37*, 1947–1956.

D'Orazio, J.A., Nobuhisa, T., Cui, R., Arya, M., Spry, M., Wakamatsu, K., Igras, V., Kunisada, T., Granter, S.R., Nishimura, E.K., et al. (2006). Topical drug rescue strategy and skin protection based on the role of Mc1r in UV-induced tanning. Nature *443*, 340–344.

Davies, H.E., and Robinson, M.J. (1963). A case of histidinaemia. Arch. Dis. Child. *38*, 80–82.

Dominiak, M., Swiecicki, L., and Rybakowski, J. (2015). Psychiatric hospitalizations for affective disorders in Warsaw, Poland: Effect of season and intensity of sunlight. Psychiatry Res. *229*, 287–294.

Dull, T., Zufferey, R., Kelly, M., Mandel, R.J., Nguyen, M., Trono, D., and Naldini, L. (1998). A third-generation lentivirus vector with a conditional packaging system. J. Virol. *72*, 8463–8471.

Espinós, C., Pineda, M., Martínez-Rubio, D., Lupo, V., Ormazabal, A., Vilaseca, M.A., Spaapen, L.J., Palau, F., and Artuch, R. (2009). Mutations in the urocanase gene UROC1 are associated with urocanic aciduria. J. Med. Genet. *46*, 407–411.

Fell, G.L., Robinson, K.C., Mao, J., Woolf, C.J., and Fisher, D.E. (2014). Skin β-endorphin mediates addiction to UV light. Cell *157*, 1527–1534.

Garwood, M., and DelaBarre, L. (2001). The return of the frequency sweep: designing adiabatic pulses for contemporary NMR. J. Magn. Reson. *153*, 155–177.

Gibbs, N.K., Tye, J., and Norval, M. (2008). Recent advances in urocanic acid photochemistry, photobiology and photoimmunology. Photochem. Photobiol. Sci. *7*, 655–667.

Hart, P.H., Gorman, S., and Finlay-Jones, J.J. (2011). Modulation of the immune system by UV radiation: more than just the effects of vitamin D? Nat. Rev. Immunol. *11*, 584–596.

Hattar, S., Lucas, R.J., Mrosovsky, N., Thompson, S., Douglas, R.H., Hankins, M.W., Lem, J., Biel, M., Hofmann, F., Foster, R.G., and Yau, K.W. (2003). Melanopsin and rod-cone photoreceptive systems account for all major accessory visual functions in mice. Nature *424*, 76–81.

Hintiryan, H., Foster, N.N., Bowman, I., Bay, M., Song, M.Y., Gou, L., Yamashita, S., Bienkowski, M.S., Zingg, B., Zhu, M., et al. (2016). The mouse cortico-striatal projectome. Nat. Neurosci. *19*, 1100–1114.

Hirata, H., Takahashi, A., Shimoda, Y., and Koide, T. (2016). Caspr3-deficient mice exhibit low motor learning during the early phase of the accelerated rotarod task. PLoS ONE *11*, e0147887.

Holliman, G., Lowe, D., Cohen, H., Felton, S., and Raj, K. (2017). Ultraviolet radiation-induced production of nitric oxide:a multi-cell and multi-donor analysis. Sci. Rep. *7*, 11105.

Hunter, J.K., and Hug, D.H. (1989). Specific inhibition of bacterial and bovine urocanases by glycylglycine. Pept. Res. *2*, 240–245.

Johnson-Huang, L.M., Suárez-Fariñas, M., Sullivan-Whalen, M., Gilleaudeau, P., Krueger, J.G., and Lowes, M.A. (2010). Effective narrow-band UVB radiation therapy suppresses the IL-23/IL-17 axis in normalized psoriasis plaques. J. Invest. Dermatol. *130*, 2654–2663.

Kalafatic, Z., Lipovac, K., Jezerinac, Z., Juretic, D., Dumic, M., Zurga, B., and Res, L. (1980). A liver urocanase deficiency. Metabolism *29*, 1013–1019.

Kamat, P.K., Kalani, A., and Tyagi, N. (2014). Method and validation of synaptosomal preparation for isolation of synaptic membrane proteins from rat brain. MethodsX *1*, 102–107.

Kammeyer, A., Pavel, S., Asghar, S.S., Bos, J.D., and Teunissen, M.B.M. (1997). Prolonged increase of cis-urocanic acid levels in human skin and urine after single total-body ultraviolet exposures. Photochem. Photobiol. *65*, 593–598.

Keller, M.C., Fredrickson, B.L., Ybarra, O., Côté, S., Johnson, K., Mikels, J., Conway, A., and Wager, T. (2005). A warm heart and a clear head. The contingent effects of weather on mood and cognition. Psychol. Sci. *16*, 724–731.

Kent, S.T., McClure, L.A., Crosson, W.L., Arnett, D.K., Wadley, V.G., and Sathiakumar, N. (2009). Effect of sunlight exposure on cognitive function among depressed and non-depressed participants: a REGARDS cross-sectional study. Environ. Health *8*, 34.

Kreitzer, A.C., and Malenka, R.C. (2008). Striatal plasticity and basal ganglia circuit function. Neuron *60*, 543–554.

Leger, M., Quiedeville, A., Bouet, V., Haelewyn, B., Boulouard, M., Schumann-Bard, P., and Freret, T. (2013). Object recognition test in mice. Nat. Protoc. *8*, 2531–2537.

Lott, I.T., Wheelden, J.A., and Levy, H.L. (1970). Speech and histidinemia: methodology and evaluation of four cases. Dev. Med. Child Neurol. *12*, 596–603.

Meldrum, B.S. (2000). Glutamate as a neurotransmitter in the brain: review of physiology and pathology. J. Nutr. *130* (4S, Suppl), 1007S–1015S.

Melo-Oliveira, R., Oliveira, I.C., and Coruzzi, G.M. (1996). Arabidopsis mutant analysis and gene regulation define a nonredundant role for glutamate dehydrogenase in nitrogen assimilation. Proc. Natl. Acad. Sci. USA *93*, 4718–4723.

Merritt, A.D., Rucknagel, D.L., Silvermanm, and Gardiner, R.C. (1962). Urinary urocanic acid in man: the identification of urocanic acid and the comparative excretions of urocanic acid and N-formiminoglutamic acid after oral histidine in patients with liver disease. J. Clin. Invest. *41*, 1472–1483.

Mitchell, S.J., and Silver, R.A. (2000). Glutamate spillover suppresses inhibition by activating presynaptic mGluRs. Nature *404*, 498–502.

Mon, A., Abé, C., Durazzo, T.C., and Meyerhoff, D.J. (2013). Effects of fat on MR-measured metabolite signal strengths: implications for *in vivo* MRS studies of the human brain. NMR Biomed. *26*, 1768–1774.

Nedergaard, M., Takano, T., and Hansen, A.J. (2002). Beyond the role of glutamate as a neurotransmitter. Nat. Rev. Neurosci. *3*, 748–755.

Parrott, W.G., and Sabini, J. (1990). Mood and memory under natural conditions: evidence for mood incongruent recall. J. Pers. Soc. Psychol. *59*, 321–336.

Radack, K.P., Farhangian, M.E., Anderson, K.L., and Feldman, S.R. (2015). A review of the use of tanning beds as a dermatological treatment. Dermatol. Ther. (Heidelb.) *5*, 37–51.

Raisová, V., and Hyánek, J. (1986). Speech disorders associated with histidinemia and other hereditary disorders of amino acid metabolism. Folia Phoniatr. (Basel) *38*, 43–48.

Rothwell, P.E., Hayton, S.J., Sun, G.L., Fuccillo, M.V., Lim, B.K., and Malenka, R.C. (2015). Input- and output-specific regulation of serial order performance by corticostriatal circuits. Neuron *88*, 345–356.

Ruegemer, J., Schuetz, B., Hermann, K., Hein, R., Ring, J., and Abeck, D. (2002). UV-induced skin changes due to regular use of commercial sunbeds. Photodermatol. Photoimmunol. Photomed. *18*, 223–227.

Scheuss, V., and Neher, E. (2001). Estimating synaptic parameters from mean, variance, and covariance in trains of synaptic responses. Biophys. J. *81*, 1970–1989.

Silver, R.A. (2003). Estimation of nonuniform quantal parameters with multiple-probability fluctuation analysis: theory, application and limitations. J. Neurosci. Methods *130*, 127–141.

Sun, Y., Nguyen, A.Q., Nguyen, J.P., Le, L., Saur, D., Choi, J., Callaway, E.M., and Xu, X. (2014). Cell-type-specific circuit connectivity of hippocampal CA1 revealed through Cre-dependent rabies tracing. Cell Rep. *7*, 269–280.

Suska, A., Lee, B.R., Huang, Y.H.H., Dong, Y., and Schlüter, O.M. (2013). Selective presynaptic enhancement of the prefrontal cortex to nucleus accumbens pathway by cocaine. Proc. Natl. Acad. Sci. USA *110*, 713–718.

Takács, V.T., Klausberger, T., Somogyi, P., Freund, T.F., and Gulyás, A.I. (2012). Extrinsic and local glutamatergic inputs of the rat hippocampal CA1 area differentially innervate pyramidal cells and interneurons. Hippocampus *22*, 1379–1391.

van den Pol, A.N., Wuarin, J.P., and Dudek, F.E. (1990). Glutamate, the dominant excitatory transmitter in neuroendocrine regulation. Science *250*, 1276–1278.

Vanhamme, L., van den Boogaart, A., and Van Huffel, S. (1997). Improved method for accurate and efficient quantification of MRS data with use of prior knowledge. J. Magn. Reson. *129*, 35–43.

Wikgren, J., Mertikas, G.G., Raussi, P., Tirkkonen, R., Äyräväinen, L., Pelto-Huikko, M., Koch, L.G., Britton, S.L., and Kainulainen, H. (2012). Selective breeding for endurance running capacity affects cognitive but not motor learning in rats. Physiol. Behav. *106*, 95–100.

Xue, T., Do, M.T., Riccio, A., Jiang, Z., Hsieh, J., Wang, H.C., Merbs, S.L., Welsbie, D.S., Yoshioka, T., Weissgerber, P., et al. (2011). Melanopsin signalling in mammalian iris and retina. Nature *479*, 67–73.

Yin, H.H., Mulcare, S.P., Hilário, M.R., Clouse, E., Holloway, T., Davis, M.I., Hansson, A.C., Lovinger, D.M., and Costa, R.M. (2009). Dynamic reorganization of striatal circuits during the acquisition and consolidation of a skill. Nat. Neurosci. *12*, 333–341.

Zamboni, N., Fendt, S.M., Rühl, M., and Sauer, U. (2009). (13)C-based metabolic flux analysis. Nat. Protoc. *4*, 878–892.

Zenobi, R. (2013). Single-cell metabolomics: analytical and biological perspectives. Science *342*, 1243259.

Zhu, H., Zou, G., Wang, N., Zhuang, M., Xiong, W., and Huang, G. (2017). Single-neuron identification of chemical constituents, physiological changes, and metabolism using mass spectrometry. Proc. Natl. Acad. Sci. USA *114*, 2586–2591.

Zielman, R., Wijnen, J.P., Webb, A., Onderwater, G.L.J., Ronen, I., Ferrari, M.D., Kan, H.E., Terwindt, G.M., and Kruit, M.C. (2017). Cortical glutamate in migraine. Brain *140*, 1859–1871.

Zurkovsky, L., Bychkov, E., Tsakem, E.L., Siedlecki, C., Blakely, R.D., and Gurevich, E.V. (2013). Cognitive effects of dopamine depletion in the context of diminished acetylcholine signaling capacity in mice. Dis. Model. Mech. *6*, 171–183.

STAR★METHODS

KEY RESOURCES TABLE

REAGENT or RESOURCE	SOURCE	IDENTIFIER
Antibodies		
Mouse monoclonal anti-HAL	Abnova	Cat# H00003034-M04,RRID:AB_566289
Rabbit anti-AMDHD1	Sigma	Cat# HPA039720, RRID:AB_10672967
Rabbit anti-UROC1	Novus	Cat# NBP1-93883, RRID:AB_11028801
Mouse monoclonal anti-GAPDH	Millipore	Cat# MAB374, RRID:AB_2107445
Mouse monoclonal anti-FTCD	Sigma	Cat# G2404, RRID:AB_477002
mouse monoclonal anti-NeuN	Millipore	Cat# MAB377, RRID:AB_2298772
Goat anti-Mouse IgG (H+L), Alexa Fluor 568	invitrogen	Cat# A-11004, RRID:AB_141371
Bacterial and Virus Strains		
pAAV-mCamKIIα-hChR2(H134R)-EGFP	Shanghai Sunbio Medical Biotechnology	N/A
siHAL	Genepharma	N/A
pHBAAV-U6-shUROC1-CMV-EGFP	Hanbio	N/A
pHBAAV-U6- shAMDHD1-CMV-EGFP	Hanbio	N/A
pHBAAV-U6- shFTCD -CMV-EGFP	Hanbio	N/A
pHBAAV-U6- shControl -CMV-EGFP	Hanbio	N/A
pAAV-CAG-EGFP	Obio Technology	N/A
Chemicals, Peptides, and Recombinant Proteins		
Picrotoxin	Sigma	P1675; CAS: 124-87-8
dimethyl sulfoxide	Sigma	v900090; CAS: 67-68-5
Tetrodotoxin	Abcam	ab120054; CAS: 4368-28-9
4-Imidazoleacrylic acid (Urocanic acid)	Sigma-Aldrich	859796; CAS: 104-98-3
1,2,3-$^{13}C_3$-Urocanic acid	Sigma-Aldrich	709638; CAS: 1173097-34-1
Histidine	Sigma	V900459; CAS:71-00-1
1-^{13}C-Histidine	Sigma-Aldrich	588644
Glycyl-Glycine	Sigma	v900403; CAS: 556-50-3
piracetam	Sangon Biotech (Shanghai)	A506285;CAS:7491-74-9
Lipofectamine 2000	Invitrogen	11668-019
avidin-biotin complex	Vector Laboratories	Cat# PK-6101, RRID:AB_2336820
3,3′-diaminobenzidine	Vector Laboratories	Cat# SK-4100, RRID:AB_2336382
Experimental Models: Cell Lines		
HEK293T cell line	Gift from Dr. Xue T lab (USTC)	N/A
Experimental Models: Organisms/Strains		
Mouse:Triple knockout (TKO)	Hattar et al., 2003	N/A
Mouse:C57BL/6J	Beijing Vital River Laboratory Animal Technology	213
Oligonucleotides		
urocanase cDNA: Forward: GAACTGGACACAACGGGG	This paper	N/A
urocanase cDNA: Reverse: CCATTGGAGACATCCCAG	This paper	N/A
Primers for genotyping of TKO mice, see Table S1	This paper	N/A
Primers for shRNA plasmid construction, see Table S2	This paper	N/A
Recombinant DNA		
Urocanase plasmids	OriGene	N/A
IPPAnase plasmids	OriGene	N/A

(*Continued on next page*)

Continued

REAGENT or RESOURCE	SOURCE	IDENTIFIER
FTCD plasmids	OriGene	N/A
pRSV-Rev	Dull et al., 1998	Addgene Cat# 12253
pMDLg/pRRE	Dull et al., 1998	Addgene Cat# 12251
pMD2.G	Gift from Didier Trono (unpublished data)	Addgene Cat# 12259
Software and Algorithms		
ImageJ	National Institutes of Health	https://imagej.nih.gov/ij/
GraphPad Prism 6	GraphPad Software	https://www.graphpad.com
jMRUI time domain analysis software package	jMRUI	http://www.jmrui.eu/welcome-to-the-new-mrui-website//
Clampfit	Molecular Devices	https://www.moleculardevices.com
Mini Analysis software	Synaptosoft	http://www.synaptosoft.com

CONTACT FOR REAGENT AND RESOURCE SHARING

Further information and requests for resources and reagents should be directed to and will be fulfilled by the Lead Contact, Wei Xiong (wxiong@ustc.edu.cn).

EXPERIMENTAL MODEL AND SUBJECT DETAILS

Mice

All animal experiments were approved by the Institutional Animal Care and Use Committee of the University of Science and Technology of China (USTC) and the Chinese Academy of Sciences (CAS). Mice were group-housed in groups of 2-5 with a 12-h light/dark cycle (lights off at 7 p.m.) and free access to food and water *ad libitum* under specific pathogen-free conditions. Male C57BL/6J mice were used for all experiments unless otherwise specified. Male triple knockout (TKO) mice (rod α transducin knockout, *Gnat*$^{-/-}$; cyclic nucleotide gated channel alpha 3 knockout, *Cnga3*$^{-/-}$; melanopsin knockout, *Opn4*$^{-/-}$) were used for sampling. The C57BL/6J mice were purchased from Beijing Vital River Laboratory Animal Technology. Genotyping of the TKO mice was performed using the primers provided in Table S1. Experimenters were blinded to all experimental conditions until all data were obtained. Unless otherwise specified, the mice were randomly assigned to control or treatment groups in all experiments.

Cell Culture

HEK293T cell line (female) was a kind gift from Dr. Xue T (USTC) and accompanied by authentication documents verifying the identity according to their short tandem repeat profiles. HEK293T cell line was cultured in Dulbecco's Modified Eagle's medium (DMEM) (HyClone) supplemented with 10% fetal bovine serum (GIBCO) at 37°C and 5% CO_2.

METHOD DETAILS

UVB Irradiation

Mice were dorsally shaved 2 days before the start of radiation exposure. During the UVB irradiation experiment, mice were kept in an acrylic chamber (15 × 30 × 50 cm) with a power-adjustable UVB lamp (G15T8E, Sankyo Denki, Japan) on top. The shaved mice were exposed to 50 mJ/cm^2 of UVB (7 μW/cm^2, 120 min) and then placed back to their home cages before testing. The irradiation intensity of UV was detected using a UV irradiometer (Photoelectric instrument factory of Beijing normal university, Beijing, China) placed on the bottom of the acrylic chamber. The suberythematic dose was determined on the basis of previous studies (D'Orazio et al., 2006; Fell et al., 2014).

Mouse Serum and Cerebrospinal Fluid (CSF) Preparation

For serum collection, the mouse blood was collected into regular 1.5 mL Eppendorf tubes and stored at room temperature for 30 min, and then centrifuged for 10 min at 4500 rpm (PICO 17, Thermo Scientific, USA) at 4°C. The supernatant was transferred to a vial and stored at −20°C until analyzed by mass spectrometry (MS).

To collect mouse CSF samples, the Isoflurane-anesthetized wild-type male C57BL/6J mice were mounted on a stereotaxic system (68015, RWD Life Science, China). After drilling through the skull, a 5 μL syringe (Hamilton) was lowered into the lateral ventricle (1.0 mm lateral, 0.3–0.5 mm posterior, 2.3–2.5 mm depth from bregma). CSF was withdrawn at a rate of 400 nL/min. Approximately 1 μL of CSF was collected per mouse.

All mouse serum (5 μl) and CSF samples were diluted 30 folds using methanol-H_2O solution (30:70, v/v). Atenolol (38-188 pM) was added as an internal standard for MS analysis.

Brain Slice Preparation

The secondary motor cortex (M_2), hippocampus (HPC), central nucleus of the amygdala (CeA), dorsal striatum (DS), nucleus accumbens (NAc) and prefrontal cortex (PFC) slices were prepared from C57BL/6J mice aged P28-P30. The mice were sacrificed and then the brains were rapidly removed from the skull and immersed in ice-cold pre-oxygenated cutting solution containing sucrose 194 mM, NaCl 30 mM, $NaHCO_3$ 26 mM, $MgCl_2$ 1 mM, glucose 10 mM, KCl 4.5 mM, and NaH_2PO_4 1.2 mM, pH 7.4. Coronal sections (300 μm) were cut using a Vibratome (VT 1200S, Leica, Germany). The tissue slices were incubated in a holding chamber containing oxygenated (95% O_2 and 5% CO_2) artificial cerebrospinal fluid (aCSF), which consisted of NaCl 124 mM, $NaHCO_3$ 26 mM, KCl 4.5 mM, NaH_2PO_4 1.2 mM, $MgCl_2$ 1 mM, $CaCl_2$ 2 mM, and glucose 10 mM (pH 7.4; osmolality, 315 mOsm/kg). For the mouse brain slices (coronal or sagittal planes) recovered from mechanical injury, they were incubated at 32°C oxygenated (95% O_2 and 5% CO_2) aCSF for approximately 30 min and then cooled to room temperature (21-23°C) at least 30 min before recording.

Single-Neuron MS

After extraction of the cell cytoplasmic chemical constituents, the capillary was coupled to the single-neuron MS, which had been fabricated as previously described (Zhu et al., 2017). After the brain slices recovered from mechanical injury, they were transferred to the recording chambers. The neurons were randomly chosen for the subsequent electrophysiological recording and MS analysis. We approached the neuron using a micromanipulator (MP-285, Sutter) and patched the neuron with borosilicate glass pipettes filled with pipette solution (NH_4HCO_3 185 mM and NH_4Cl 80 mM) by applying negative pressure. The neurons were clamped at –70 mV after the patched cell membrane was broken by rapidly applied negative pressure. After the electrophysiological data were recorded, the cytoplasmic chemical constituents were obtained from the assayed neuron by applying negative pressure. Only neurons with tightly held seals (> 1 GΩ) and nonruptured membranes were selected for analysis, avoiding the dilution of intracellular fluid by aCSF. Once a sufficient amount of fluid was withdrawn from the cell, the patch pipette was quickly removed from the slice and then assayed via MS.

An AC voltage with an amplitude of 4 kV at ~500 Hz was applied outside of the spray capillary micropipette. The tip of the spray micropipette was kept ~5 mm away from the orifice of the MS instrument. High resolution mass measurements were analyzed using an Exactive plus MS instrument (Thermo Fisher Scientific, San Jose, CA, USA). Its main experiment parameters were set as follows: Capillary temperature, 275°C; S-lens radio frequency (RF) level, 50%; mass resolution, 70,000; maximum inject time, 10 ms; and microscan, 1. Other MS experiments were conducted with a LTQ Velos Pro. MS instrument (Thermo Fisher Scientific, San Jose, CA, USA). MS parameters were capillary temperature 275°C, S-lens RF level 42%, maximum injection time 300 ms, and microscan 1. Chemical structure were confirmed by tandem MS using LTQ Velos Pro. MS instrument based on collision-induced dissociation (CID) with helium (He) as background gas at 28% energy. Commercial electrospray ionization (ESI) source was removed before our experiments. Positive ion mode was used in our experiments.

^{13}C-Isotope Tracing Experiments

To trace HIS metabolism, 1-^{13}C-HIS was added into aCSF at a final concentration of 3 mg/ml. After the mouse brain slices (coronal or sagittal planes) recovered from mechanical injury, they were transferred to oxygenated aCSF with or without 1-^{13}C-HIS and incubated for 1 h at room temperature. After the mouse slices incubated with aCSF containing 1-^{13}C-HIS, they were washed three times with oxygenated aCSF at room temperature and then transferred to the recording chambers. Other experimental procedures were the same as those for single-neuron MS.

To trace UCA metabolism *in vivo*, we intravenously (i.v.) injected 1,2,3-$^{13}C_3$-UCA (20 mg/kg, 2.5 mg/ml) diluted in saline into the mice 30 min before serum/CSF collection and brain slices preparation. Saline is the corresponding vehicle solution. All the collected samples were analyzed using MS. All drug treatment or control groups were blinded from experimenters.

Calibration Curves of UCA

Estimations of intracellular UCA levels in neurons were calculated from calibration curves with external UCA standards at concentrations ranged from 1 μM, 10 μM, 100 μM and 300 μM with three replicates per concentration point. All calibrations were obtained with artificial intracellular solution: potassium gluconate 130 mM, NaCl 6 mM, ethylene glycol-bis(β-aminoethyl ether)-N,N,N′,N′-tetraacetic acid (EGTA) 11 mM, 4-(2-Hydroxyethyl)piperazine-1-ethanesulfonic acid (HEPES) 10 mM, $CaCl_2$ 1 mM, NaOH 4 mM, $MgCl_2$ 1 mM, Mg-ATP 2 mM and Na-GTP 0.2 mM (pH was adjusted to 7.3).

Lentivirus Production and Transduction

HEK293T cells in a 10-cm plate were seeded at 70% confluence 1 day before transfection. The cells were transfected the next day at 85% confluence with 6 μg of plasmid containing *Uroc1* shRNA or control shRNA, 6 μg of pRSV-Rev, 6 μg of pMDLg/pRRE and 3 μg of pMD2.G (Addgene) together with 21 μL of Lipofectamine 2000 (Invitrogen). The medium was replaced 10 h after transfection. Viral supernatant was harvested 70 h post-transfection, filtered with a 0.45-μm filter (Millipore), and centrifuged for 2.5 h at 30,000 g 4°C. After centrifugation, the supernatant was removed and the pellet was resuspended with 20 μL of PBS containing 10% FBS and 8 μg/μl polybrene and stored at −80°C.

RNA Interference

Small interfering RNA (siRNA) were used for histidase knockdown. HEK293T cells were co-transfected with either targeting siRNA or control siRNA (Genepharma) and histidase overexpressing plasmid (OriGene) using lipofectamine 2000 reagent for 48 h. For knockdown of urocanase, IPPAnase or FTCD, short hairpin RNA (shRNA) plasmid constructs (Hanbio) were co-transfected with overexpressing plasmids of urocanase, IPPAnase or FTCD (OriGene) into HEK293T cells for 48 h. The subsequent western blotting analysis were performed to validate the knockdown efficacy of siRNA or shRNA. The most efficient shRNA plasmid construct was used to package AAV virus (Hanbio) for *in vivo* knockdown of urocanase, IPPAnase or FTCD. Several independent siRNA duplexes or shRNA plasmid constructs were used and the sequence were listed in Table S2.

Synaptosomal Preparation

Mouse brain synaptosomes were prepared as previously described (Kamat et al., 2014). Briefly, the mice were anaesthetized and perfused with ice-cold saline. The brain was removed and kept on ice-cold 0.32 M sucrose HEPES buffer (NaCl 145 mM, KCl 5 mM, $CaCl_2$ 2 mM, $MgCl_2$ 1 mM, glucose 5 mM, HEPES 5 mM, pH 7.4) supplemented with protease inhibitor cocktail. Tissue was homogenized using a Dounce homogenizer and the homogenate was centrifuged at 800 g, 4°C, 10 min to collect the supernatant (S1). The supernatant (S2) containing cytosol was collected for electrophoresis after the S1 was centrifuged at 10,000 g, 4°C, 20 min. The pellet (P2) containing synaptosomes were suspended in 0.8 M sucrose HEPES buffer solution and further centrifuged at 20,000 g, 4°C, 30 min. The pellet was washed in HEPES buffer twice and were suspended in lysis buffer solution (Tris 50 mM, NaCl 150 mM, 1% NP-40, 0.5% Sodium dexyocholate supplemented with protease inhibitor cocktail as the synaptosome). The synaptosomal preparation was used for western blotting analysis.

Western Blotting

HEK293T cells co-transfected with overexpressing plasmids and shRNA plasmids were collected and lysed in lysis buffer solution. Mouse brain tissues were homogenized and sonicated followed by centrifugation at 10,000 g, 4°C for 30 min. The supernatants were diluted 1:1 with laemmli 2X sample buffer and denatured at 99°C for 10 min. The samples were separated on 12% SDS/PAGE gels. After electro-transferring to a 0.45 μm PVDF membrane, the membrane were blocked in 5% BSA and blotted with following antibodies: anti-HAL (Abcam, 1:500), anti-UROC1 (Novus, 1:250), anti-AMDHD1 (Sigma, 1:250) and anti-GAPDH (Millipore, 1:40000). HRP-conjugated secondary antibodies and chemiluminescent substrate (Thermo Fisher) were used to detect signals.

Brain Tissue Preparation and Immunohistochemistry

Mice (N = 3) were deeply anesthetized by intraperitoneal (i.p.) injection of pentobarbital (40 mg/kg), and then perfused with chilled PBS, followed by 4% paraformaldehyde (PFA) in PBS. Brains were removed and immersed in the same fixative solution (4% PFA in PBS) overnight, then were subsequently incubated in 30% (wt/vol) sucrose in PBS for 24 h at 4°C. Sagittal brain sections 40 μm thick were prepared using a cryostat (CM 1860, LEICA Microsystems) at −20°C and collected into a 12-well plate.

After a PBS wash (three times within 5 min), sections were incubated for 20 min in 3% peroxide mixed in methanol in order to inactivate the endogenous peroxidase. Sections were incubated with 0.3% Triton X-100 and 5% normal goat serum in PBS. After 40 min of blocking, the sections were incubated with rabbit anti-Histidase antibody (1:200, ab154063, Abcam), anti-urocanase antibody (1:200, NBP1-93883, Novus), or anti-IPPAnase antibody (1:200, HPA039720, Sigma) in PBS for 24 h at 4°C. On the following day, the sections were washed in PBS and incubated with biotinylated goat anti-rabbit (1:1000, PK-6101, Vector Laboratories) for 2 h. After a PBS wash, sections were reacted with avidin-biotin complex (ABC, PK6101, Vector Laboratories) for 30 min. Brain sections were washed with PBS and collected on gelatin-coated slides, air-dried. Slides were incubated with 3,3′-diaminobenzidine (DAB, SK-4100, Vector Laboratories) for 2-4 min before a distilled-water wash. Slides were dehydrated in alcohol gradient (90, 95, 100%), immersed in xylene, mounted with Neutral Balsam (E675007, Sangon Biotech). All the incubations were done at room temperature, unless mentioned otherwise.

Fluorescent *in Situ* Hybridization (FISH) Experiment

For FISH, the detected fragment of mouse urocanase cDNA was cloned into pEASY-T3 with the pair of primers provided in the Key Resources Table. Probes were prepared with DIG RNA Labeling Mix (Roche) by *in vitro* transcription with T7 or SP6 polymerases. Frozen sections with 15 μm thick were collected on PLL-coated slides, then further fixed in 4% PFA/ PBS for 10 min, subsequently washed with DEPC-PBS for 10 min, and then treated with 3% H_2O_2 to block the endogenous peroxidase activity. After that the slides were treated with 0.5% Triton X-100/DEPC-PBS for 20 min, at last acetylated with 0.25% acetic anhydride in 0.1 M triethanolamine (pH 8.0). After acetylation, the sections were prehybridized for 2 h at 60°C, and then hybridized for with either scrambled or positive probe for 16 h at 60°C. After washing twice in 2 × SSC at 60°C for 15 min each, the samples were treated with 5 μg/ml RNase A at 37°C. They were sequentially washed twice in 0.2 × SSC at 60°C for 30 min each. Probes were detected by standard method using anti-Digoxigenin-POD Fab fragments (Roche) and TSA-Plus Cyanine 3 system (PerkinElmer).

Detected sequence:

gaactggacacaacgggggaactcttggtggacctcgggtcagaccagacatcctgtcacaacccgttcaatggcggctactaccctgtgcagctcagcttctcagaggcc
cagagcctcatgtcctccaaccctgctgccttcaagcacctggtgcaggaaagcctgaggaggcatgtcgcagccatcaacaggttggcccaagagaagttcttcttctggg
actatggtaatgccttcctcttggaggctcagagagcaggagcagatgtagagaagaaaggagccaacaagatggagttccgctacccctcctatgtccagcacattatggg
ggatatattctcccagggctttgggcccttccgctgggtatgcacatcaggggacccccaggacctggctgtcactgatcatctggccacatctgtactggagaaagccattg
ctgatggagtgaaggcatctgtgaagctacagtatatggataatatacgctggatccgagaggctgccaagcatcagctggtggtgggctcccaggcaaggatcctgtactc
agaccagaaaggccgtgtggccattgctgtggccattaaccaggccatcgccagtgggaagatcaaggcaccagtggtcctgagccgtgaccaccatgatgtgagtggca
ctgacagccccttcagggagacttcgaatatttatgacggttctgccttctgcgcagacatggccgtgcagaacttcgtgggagatgcctgtcgtggtgccacctgggttgcac
ttcacaatggaggggtgtaggctggggtgaagtcatcaatgggggatttggccttgttctagatggaactgcagaggctgagcagaaagccaggatgatgctcagctggga
tgtctccaatgg.

Magnetic Resonance Imaging Experiments

Male mice aged 8-10 weeks were used. The integrated animal/MRI facility at high magnetic field laborary allowed for the measurements to be taken without requiring the mice to be euthanized at the end of experiment, and all animals were returned to the animal facility after they had fully recovered from the experimental procedures.

All magnetic resonance imaging (MRI) experiments were performed on a 9.4 Tesla 40-cm horizontal bore MR spectrometer (Agilent Technologies, Santa Clara, CA, USA). The animals were placed in a prone position on a specially designed cradle and inserted into the magnet. A home-built radiofrequency (RF) coil were used for both RF transmission and signal detection. Mice were anaesthetized with isoflurane (3.5% induction, 1.5%–2.0% maintenance in air/O_2 2:1) for the duration of the scan (approximately 2.5 h). Respiratory rate and rectal temperature were monitored throughout the experiment with a physiologic monitoring unit (model 1030; SA Instruments, Stony Brook, NY), and the body temperature was maintained at 36.5°C with a homemade heating pad. Reference T_2-weighted images were acquired, from which the spectroscopic region of interest were determined in the cortical M_2 area as well as the HPC CA3 area. Subsequently, the i.v. injection of UCA (20 mg/kg, 2.5 mg/ml diluted in saline) began at a constant rate of 100 μl/min through the tail vein with a syringe micro-pump, and the procedure was completed within 2 min. MR spectra were acquired at 0 min, 20 min, 40 min, 60 min, 80 min and 100 min post-injection of UCA solution.

T_2-weighted MR images were acquired using a fast spin echo sequence with a repetition time (TR) of 5000 ms, echo spacing = 10 ms, echo train length (ETL) = 4; additionally, localized proton spectra from the M_2 and HPC regions outlined on the T_2-weighted images were acquired using the following parameters: effective echo time (TE) = 30 ms, field of view (FOV) = 16 × 16 mm^2, matrix size = 192 × 192, slice thickness = 1 mm (10 slices, gap = 0), and bandwidth (BW) = 25 kHz. A LASER (Localization by Adiabatic Selective Refocusing) sequence (Garwood and DelaBarre, 2001) was used in this study. The acquisition parameters were: TR/TE = 2000/36 ms, voxel size = 1 × 1 × 2 mm^3, spectral width = 4006 Hz, and Free induction decay size = 4096 with 512 averages. Typical spectra line widths for water resonance after 3D shimming were approximately 20 Hz.

Electrophysiological Recording

Slices were transferred into the recording chamber continuously perfused at 3-4 ml/min with aCSF at 28°C. Neurons were visualized using a fixed-stage microscope (BX50WI, Olympus, Tokyo, Japan) with differential interference contrast and infrared illumination. We obtained all whole-cell voltage clamp mode recordings using borosilicate glass pipettes (5-7 MΩ) filled with internal solutions. The internal solution (pH 7.2) for excitatory postsynaptic currents (EPSC) recording contained K-gluconate 145 mM, HEPES 5 mM, Mg-adenosine triphosphate (ATP) 5 mM, Na-guanosine 5′-triphosphate (GTP) 0.2 mM, and EGTA 10 mM. The miniature excitatory postsynaptic currents (mEPSCs) were recorded with a holding potential of −70 mV and PTX (100 μM), which was used to block the inhibitory neurotransmitter receptors ($GABA_A$ and glycine receptors), diluted with aCSF. For mEPSC experiments, brain slices from C57BL/6J mice expressing pAAV-mCamKIIα-hChR2(H134R)-EGFP in M_2 or HPC CA3 were cut for ChR2 stimulation test. Dorsal striatum neurons or HPC CA1 neurons were recorded with single optical stimulation of $GLU^{M2\rightarrow DS}$ or $GLU^{CA3\rightarrow CA1}$ projecting axons, respectively. Only neurons respond to a 473-nm laser (AniLab-Opto, 10 mW/mm^2) were selected for the following tests. The mEPSCs were collected after TTX (final concentration: 0.5 μM) was added to the bath perfusion. To measure presynaptic glutamate release of M_2-DS or HPC CA3-CA1 circuit, the multiple probability fluctuation analysis was used as previously described (Scheuss and Neher, 2001; Silver, 2003; Suska et al., 2013). Briefly, a train of five light pulses at 20 Hz frequency and 5-ms duration was used to stimulate the ChR2-expressing axons every 10 s. 50-100 evoked EPSCs were recorded at five release probability conditions. Experimental results were discarded if the series resistance varied by more than 15% or exceeded 25 MΩ.

AMPA/NMDA Ratio Measurement

To evoke EPSC currents in hippocampal CA1 pyramidal neurons, Schaffer collateral was stimulated using a concentric circular electrode every 20 s. PTX (100 μM) was diluted with aCSF to block the inhibitory neurotransmitter receptors ($GABA_A$ and glycine receptors). CA1 Pyramidal neurons were voltage-clamped at −70 and +40 mV to record AMPAR-mediated and NMDAR-mediated currents respectively. For each neuron, the total 10 sweeps of AMPAR and NMDAR-mediated currents were recorded and the average value of currents were then calculated. The NMDAR-mediated current was measured at 50 ms after the stimulation. The

AMPAR-mediated current was measured as the peak value. Then, the AMPA/NMDA ratio was calculated by dividing average AMPA EPSC by NMDA EPSC.

Stereotaxic Surgery, Cannula Placement and Microinjection

Mice were anaesthetized with pentobarbital sodium (i.p., 0.5%, 0.01 ml/g) and placed on a stereotaxic apparatus (68015, RWD Life Science, China). Ophthalmic ointment was applied to prevent the eyes from drying. A midline scalp incision was made, and a craniotomy was drilled above each cannula implantation or injection site. For local drug infusion, guide cannula (62001, RWD) were implanted into lateral ventricles (anteroposterior, A/P: −0.3 mm; medio-lateral, M/L: −1.0 mm; dorsoventral, D/V: −1.8 mm). The glycyl-glycine (GG) was dissolved in saline (13.2 μg/μl, 0.9% NaCl). Thirty min before the experiment, infusion needles attached to 10 μL syringes were inserted into the guide cannula, and 1 μL of GG solution was delivered within 2 min. For lentiviral shRNA or pAAV-mCamKIIα-hChR2(H134R)-EGFP injection, glass micropipette attached to 10 μL syringes were placed bilaterally into the M_2 cortex (A/P: +1.3 mm; M/L: 0.7 mm; D/V: −0.8 mm) or the CA3 region of the hippocampus (A/P: −1.7 mm; M/L: 2.2 mm; D/V: 2.25 mm), and 0.5 μL of virus was infused per side at a rate of 50 nl/min using a pump (Legato130, KD Scientific). Mice were allowed to recover for 2 weeks before behavioral tests or electrophysiological recordings. For fluorescence imaging, we injected 0.5 μL of AAV-CAG-EGFP (1.6×10^8 vg/ml, Obio Technology) into the CA3 and waited 3 weeks

Immunofluorescence after Intracerebroventricular (ICV) administration of GG

For NeuN immunofluorescence, after 2-h ICV injection of GG or saline, male C57BL/6J mice from both groups (N = 3 mice each group) were deeply anesthetized by pentobarbital (i.p., 40 mg/kg), and then perfused with chilled PBS, followed by 4% PFA in PBS. Brains were collected and immersed in 4% PFA in PBS overnight, then were subsequently incubated in 30% (wt/vol) sucrose in PBS for 24 h at 4°C as above described. Coronal brain sections (40 μm) were prepared using a cryostat (CM 1860, LEICA Microsystems) at −20°C and collected into a 12-well plate. After a PBS wash (three times within 5 min), sections were incubated for 20 min in PBS containing 10% goat serum and 0.3% Triton X-100.Then slices were incubated with mouse anti-NeuN antibody (1:200, Millipore) at 4°C overnight. The slices were then incubated with goat anti-mouse secondary antibody conjugated with alexa 568 (1:1000, invitrogen) for 1 h at room temperature. After washing with PBS for three times, slices were sealed for imaging. Immunofluorescence-labeled images were examined by confocal microscopy (LSM 880, Olympus).

Motor Learning

We used the rotarod training system (XR1514, Xinruan, Shanghai, China) to test the motor skill learning of mice as previously described (Hirata et al., 2016; Wikgren et al., 2012). Before the first training sessions, the mice were habituated to stay on a stationary rod for 2 min. To assess motor learning, a total of six trials for the rotarod test were carried out using an accelerating protocol from 4 to 60 rpm in 300 s with 20-min inter-trial intervals. Three training sessions every day were performed for 2 days. After falling, the mice were immediately placed back to their home cages, and the time to fall was automatically recorded by the rotarod software. The mice were taken from the rod and the latency was recorded as 300 s, if stayed on the rotarod more than the full 300 s of a trial. The apparatus and testing area were cleaned with 75% ethanol, when the trials were finished.

Novel Object Recognition

Novel object recognition methods have been described previously (Leger et al., 2013; Zurkovsky et al., 2013). Briefly, the open-field apparatus consisted of an acrylic chamber (40 × 40 × 30 cm). Two different objects were prepared in duplicate: towers of Lego bricks (12.5 cm high, 2.5 cm deep and 7.5 cm wide, built from blue, yellow, red and green bricks) and Falcon tissue culture flasks (15.5 cm high, 3.5 cm deep and 9 cm wide, transparent plastic with an orange bottle cap). The objects were placed 5 cm away from the walls and attached to the floor. Mice were tested during the dark phase (active phase between 7:00 p.m. and 7:00 a.m.). Before training, mice were placed in the training room for 30 min. During the familiarization session, mice were allowed to freely explore two identical objects (Lego bricks) placed into the arena at fixed locations for 3 min. The ANY-maze video-tracking system (Stoelting, Wood Dale, USA), which is based on nose-point detection, was used to record the time spent exploring objects. Active exploration was defined as mice sniffing or touching the object when the gap between the nose and the object was less than 2 cm. Climbing over the object or gnawing the object was not considered as exploratory activity. At the end of the test, each mouse was returned to its home cage, and the chamber and objects were cleaned using 75% ethanol, then air-dried for 3 min. After an intersession interval (ISI) of 2 or 24 h, one of the familiar objects was replaced by a novel object (Falcon tissue culture flasks). The location of the novel object (left or right) was randomized among the mice and the groups tested. Object preference was calculated by using the following formula: preference % = (time to explore the individual object/total exploration time for both objects) × 100%). Data were excluded if the total of exploration time was less than 10 s.

QUANTIFICATION AND STATISTICAL ANALYSIS

Statistical analysis was performed using GraphPad Prism 6 (GraphPad Software). Paired and unpaired two-tailed Student's t tests were used to compare difference between treatment and control groups and *P value*s were plotted ($p < 0.05$ was considered as statistically significant difference). Results are expressed as mean ± SEM (standard error of the mean). The number (N) of mice or cells,

the statistical approaches used and statistical significance are indicated in the Figures and Figure legends. For single-neuron MS and electrophysiological recording experiments, N = number of neurons collected from at least 3 mice. For mouse serum or CSF experiments, western-blot, immunohistochemistry and behavioral experiments, n = number of mice. Sample sizes were determined based on previous experience. No statistical methods were used to predetermine sample size. The main authors of this manuscript re-calculated independently all the results of every experiment. All the data collected from control and experimental groups in our experiments were analyzed blindly. More information concerning data quantification and analysis for different experiments can be found below.

MS Data Analysis

Metabolites identification was based on high resolution mass measurements, isotopic profiles and matching tandem mass spectral data from endogenous substances with chemical standards when available. For high resolution mass measurements, to exclude data with faulty assignments, mass deviation was set lower than 15 ppm. For analysis of ^{13}C-labeling results, the $\Delta(^{13}C/^{12}C)(\%)$ is defined and calculated by the following formula:

$$\Delta(^{13}C/^{12}C)(\%) = \frac{Intensity\ of\ ^{13}C-M}{Intensity\ of\ M}_{(^{13}\text{C-labeled group})} - \frac{Intensity\ of\ ^{13}C-M}{Intensity\ of\ M}_{(\text{non-}^{13}\text{C-labeled group})}$$

Where M represents HIS, UCA, IPPA, FMGA or GLU.

MR Spectra Analysis

All MR spectra were processed using the jMRUI time domain analysis software package (http://www.jmrui.eu/welcome-to-the-new-mrui-website/). Preprocessing steps consisted of exponential apodization at 5 Hz, Fouriers transformation and phase correction of the transformed spectrum. The chemical shifts of metabolite peaks were referenced to the N-acetylaspartate CH_3- group at 2.02 ppm. AMARES (advanced method for accurate, robust and efficient spectral fitting) (Vanhamme et al., 1997), a widely used quantitation tool for MRS data, was employed to fit the spectra and quantify the GLU signal, using the none-suppressed water peak in spectra as intensity reference to quantify metabolite concentration (Mon et al., 2013).

Electrophysiological Data Analysis

The electrophysiological data were acquired using an Axon MultiClamp 700B amplifier (Molecular Devices, AXON), filtered at 3 kHz and digitized at 10 kHz using an Axon Digidata 1500A digitizer combined with pCLAMP 10.4 software. Data detection was accomplished using Mini Analysis software. For variance-mean analysis (multiple probability fluctuation analysis), 50-100 light-evoked EPSCs were averaged and variance of peak EPSCs was calculated. Variance plotted against the mean amplitude of EPSCs for each eliciting condition. We used a binomial model to calculate the following parameter as described previously (Suska et al., 2013).

$$I = NPrQ \quad [S1]$$

$$\sigma^2 = NQ^2Pr(1-Pr) \quad [S2]$$

Fitting curve indicated that the variance (σ^2) of EPSC amplitudes has a parabolic relationship with I. Quantal size (Q) is equal to the slope of the best fit line in a synapse with low release probability (Pr). The number of synapses (N) and Pr were calculated with [S1] and [S2]. Neurons not fitted were discarded for data analysis.

Western Blot Analysis

The intensity of the bands revealed in western blot photographic films was quantified using the gel quantification plugin on ImageJ software. Absolute values were normalized to the intensity of loading control (GAPDH) bands from the same samples. Results are expressed as the normalized values of band intensity relative to GAPDH.

Immunofluorescence Analysis

For all Immunofluorescence quantifications, at least 3 to 6 coronal brain slices per mouse from at least 3 independent mice were analyzed. Serial sections of several brain regions were immunostained and the number of NeuN-positive neurons in the field of view (FOV) was counted by ImageJ software.

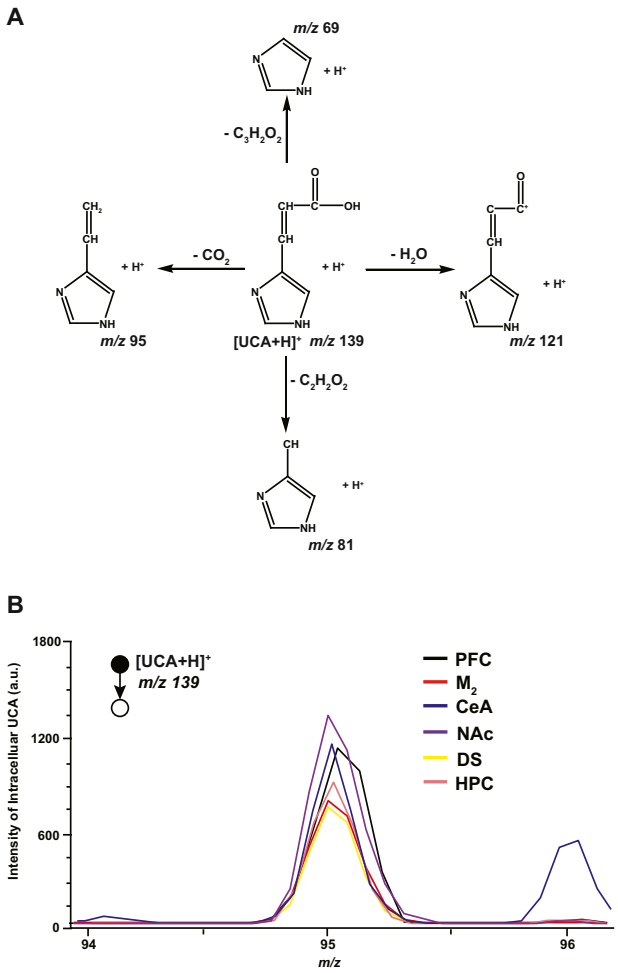

Figure S1. Detection of Urocanic Acid in the Neurons from Several Brain Regions, Related to Figure 1

(A) The possible fragment pathway of protonated UCA in collision induced dissociation.

(B) Representative tandem mass (MS/MS) spectra of intracellular UCA in single neurons from brain regions of prefrontal cortex (PFC), secondary motor cortex (M_2), central nucleus of the amygdala (CeA), nucleus accumbens (NAc), dorsal striatum (DS) and hippocampus (HPC) of mice.

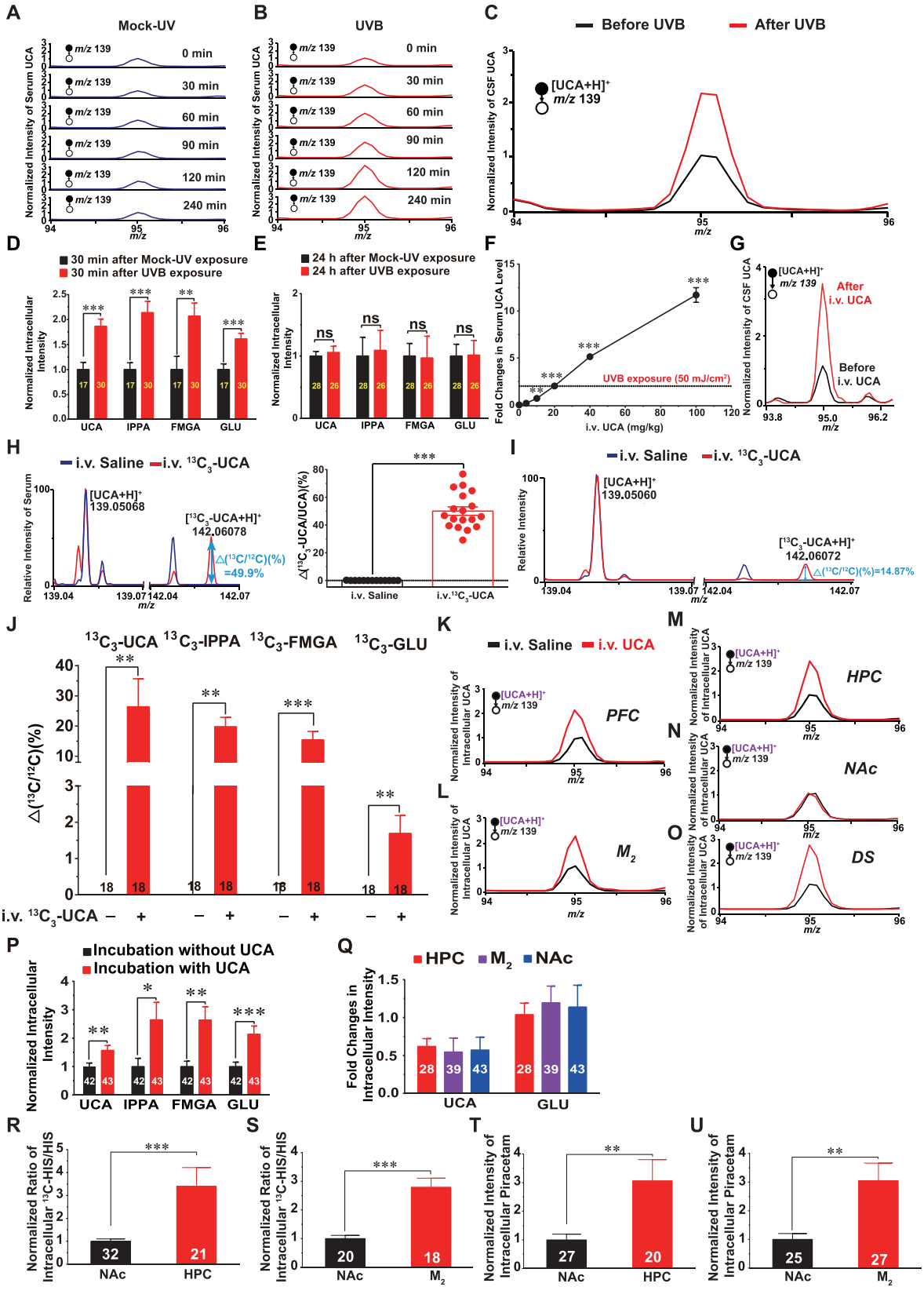

(legend on next page)

Figure S2. Effects of UVB Exposure and i.v. UCA Administration on UCA Levels in the Serum, CSF, and Single Neurons, Related to Figure 2

(A and B) Representative MS/MS spectra of UCA in mouse serum at 0, 30, 60, 90, 120 and 240 min after mock-UV (A) or UVB exposure (B). All spectra were normalized to their respective controls (0 min, mock-UV).

(C) Representative MS/MS spectra of UCA in mouse cerebrospinal fluid (CSF) before and after UVB exposure. All spectra were normalized to control group (before UVB).

(D and E) The normalized intensities of intracellular UCA, IPPA, FMGA and GLU in neurons of HPC from mice 30 min (D) or 24 h (E) after mock-UV or UVB exposure.

(F) The fold changes in MS intensity of serum UCA at 0.5 h after i.v. injection of UCA at 4, 10, 20, 40 and 100 mg/kg (N = 3 mice per dose). The dotted line indicates the fold changes in mouse blood UCA level after 2-h UVB exposure (50 mJ/cm^2).

(G) Representative MS/MS spectra of UCA in mouse CSF before (black line) and after (red line) i.v. injection of UCA (20 mg/kg, 30 min). All spectra were normalized to the control group (before i.v. UCA).

(H) Representative MS spectra of UCA and 1,2,3-$^{13}C_3$-UCA in mouse serum after i.v. injection of saline (blue line) or 1,2,3-$^{13}C_3$-UCA (red line, 20 mg/kg, 30 min). The spectra of $^{13}C_3$-UCA were normalized to the spectra of UCA. The 1,2,3-$^{13}C_3$-UCA /UCA ratios in the mouse serum after i.v. injection of saline or $^{13}C_3$-UCA (20 mg/kg, 30 min).

(I) Representative MS spectra of UCA and 1,2,3-$^{13}C_3$-UCA in mouse CSF after i.v. injection of saline or 1,2,3-$^{13}C_3$-UCA (20 mg/kg, 30 min). The spectra of $^{13}C_3$-UCA were normalized to the spectra of UCA.

(J) Identification of the *in vivo* UCA-GLU metabolic pathway in single HPC neurons via ^{13}C-labeling assay. The ^{13}C-UCA/UCA, ^{13}C-IPPA/IPPA, ^{13}C-FMGA/FMGA and ^{13}C-GLU/GLU ratios in single neurons from the HPC of mice with or without i.v. injection of ^{13}C-UCA (20 mg/kg, 1 h).

(K-O) Representative MS/MS spectra of intracellular UCA in single neurons from brain regions of PFC (K), M_2 (L), HPC (M), NAc (N) and DS (O) with i.v. injection of UCA (20 mg/kg, 30 min) or saline. All spectra were normalized to their respective controls (i.v. saline group).

(P and Q) Effects of UCA-incubation on intracellular level of UCA and related metabolites in NAc neurons. (P) Normalized intensities of intracellular UCA, IPPA, FMGA and GLU in single HPC neurons with or without UCA preincubation (0.7 mg/ml). Data were normalized to their respective controls (neurons without UCA-incubation). (Q) Fold changes in intracellular intensities of UCA and GLU in neurons from HPC, M2 and NAc brain slices after UCA preincubation (0.7 mg/ml).

(R–U) Comparison of the permeability of BBB for exogenous small molecules in NAc. (R) The normalized ^{13}C-HIS/HIS ratios in single neurons from the NAc and HPC after i.v. injection of ^{13}C-HIS (10 mg/kg, 30 min). (S) The normalized ^{13}C-HIS/HIS ratios in single neurons from the NAc and M_2 after i.v. injection of ^{13}C-HIS (10 mg/kg, 30 min). (T) The normalized intensities of intracellular piracetam in single neurons from the NAc and HPC after i.v. injection of piracetam (2 mg/kg, 30 min). (U) The normalized intensities of intracellular piracetam in single neurons from the NAc and M_2 after i.v. injection of piracetam (2 mg/kg, 30 min). All data were normalized to NAc group.

All digits within the columns represent numbers of total neurons measured from 3 mice. Data are represented as mean ± SEM. *$p < 0.05$, **$p < 0.01$, ***$p < 0.001$ based on unpaired t test.

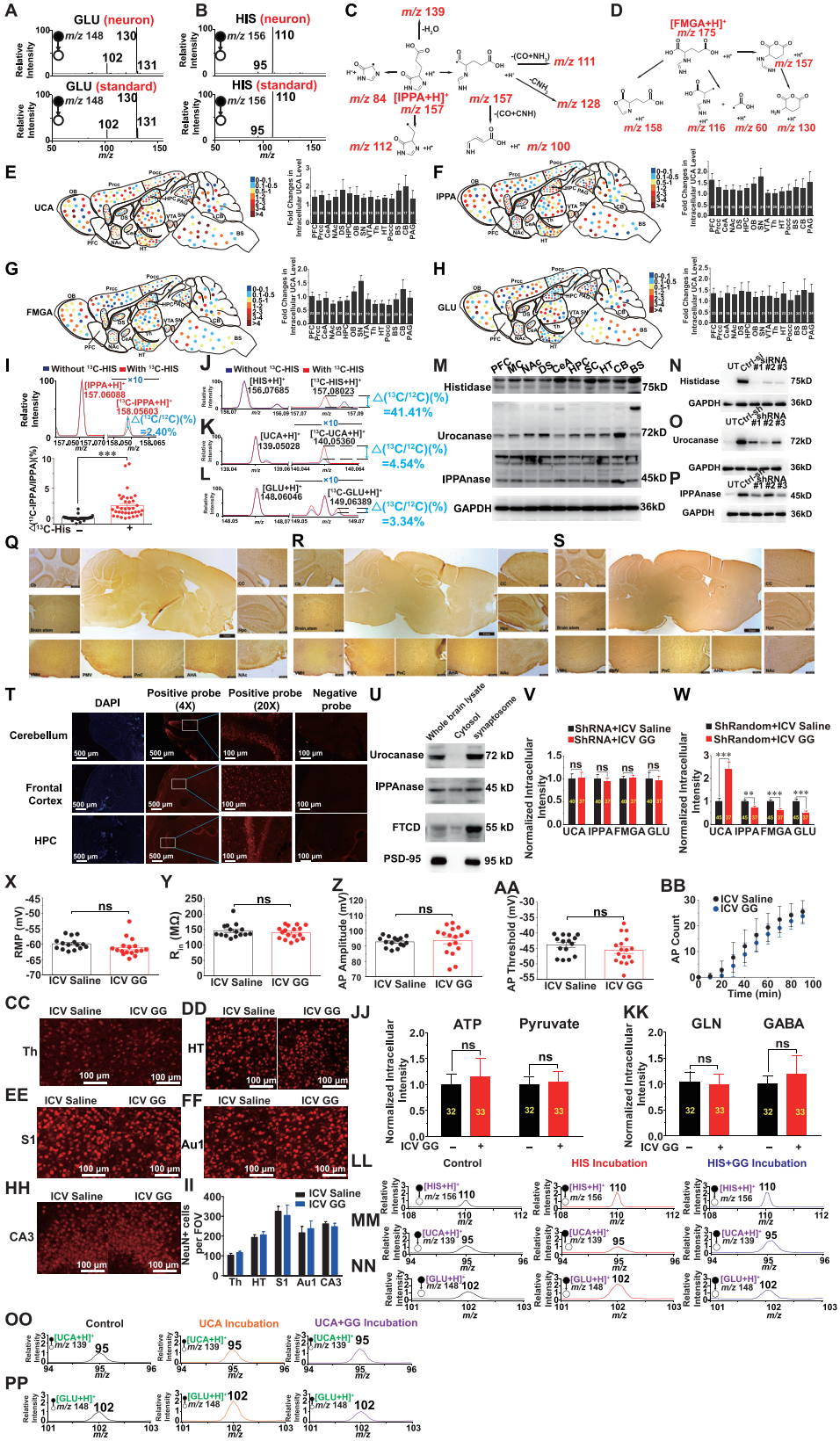

(legend on next page)

Figure S3. Identification of the HIS-UCA-GLU Metabolic Pathway in Neurons of Various Brain Regions in Mice, Related to Figure 3

(A and B) Representative MS/MS spectra for intracellular glutamate (GLU) (A, top) and histidine (HIS) (B, top) from single HPC neurons and standards of GLU (A, bottom) and HIS (B, bottom).

(C and D) The possible fragment pathway of protonated 4-Imidazolone-5-propionic acid (IPPA) (C) and formiminoglutamic acid (FMGA) (D) in collision induced dissociation.

(E–H) The heatmap of HIS-incubation-induced increases in the intracellular level of metabolites involved in the HIS-UCA pathway in the brain. Sagittal mouse brain slices were incubated with HIS at 0.2 mg/ml for 1 h or artificial cerebrospinal fluid (aCSF) as a control. Each dot represents a measured neuron at the approximate position in the brain slice. The color of each dot represents the range of fold changes in the intracellular level of UCA (E), IPPA (F), FMGA (G) or GLU (H) in neurons from the brain slice after HIS incubation, when compared to the adjacent brain slice incubated with control aCSF. Please be aware that the brain regions in this map are artificially flattened within the same plane for viewing convenience. The bar graphs in the right portion indicate the average values of HIS-incubation-induced fold changes in intracellular levels of UCA (E), IPPA (F), FMGA (G) or GLU (H) in the neurons from certain brain regions. OB (Olfactory bulb, M/L:-0.6); PFC (Prefrontal cortex, M/L:-0.48); Prcc (Precerebral cortex, M/L:-0.84); Pocc (Posterior cerebral cortex, M/L:-0.96); DS (Dorsal striatum, M/L:-1.08); NAc (Nucleus accumbens, M/L:-0.96); HPC (Hippocampus, M/L:-1.08); Th (Thalamus, M/L:-0.84); HT (Hypothalamus, M/L:-0.24); CeA (Central amygdaloid nucleus, M/L:-2.4), VTA (Ventral tegmental area, M/L:-0.6); SN (Substantia nigra, M/L:-0.6); PAG (Periaqueductal gray, M/L:0.48); BS (Brain stem, M/L:0.48); CB (Cerebellum, M/L:-0.6). M/L: medio-lateral.

(I) (Top) Representative MS spectra of IPPA and ^{13}C-IPPA in single HPC neurons with or without preincubation of ^{13}C-HIS (3 mg/ml, 1h). The spectra of ^{13}C-IPPA were normalized to the spectra of IPPA either without (blue line) or with (red line) ^{13}C-HIS incubation. x10: the signal is magnified ten times. (Bottom) Differential ratio of intensity of intracellular ^{13}C-IPPA/IPPA with or without preincubation of ^{13}C-HIS (3 mg/ml, 1 h).

(J–L) Representative MS spectra of HIS and ^{13}C-HIS (J), UCA and ^{13}C-UCA (K), GLU and ^{13}C-GLU (L) in the single HPC neurons without or with preincubation of ^{13}C-HIS (3 mg/ml, 1h). The spectra of ^{13}C-HIS, ^{13}C-UCA and ^{13}C-GLU were normalized to the spectra of HIS, UCA and GLU separately either without (blue line) or with (red line) ^{13}C-HIS incubation. x10: the signal is magnified ten times.

(M) Full images of Western-blot for Figure 3F.

(N–P) Validation of antibodies by western blot analysis of overexpressed histidase (N), urocanase (O) and IPPAnase (P) 48 h after siRNA or shRNA transfection in HEK293T cells. UT: untransfected cells; Ctrl-si: random control siRNA; Ctrl-sh: random control shRNA.

(Q–S) The immunohistochemistry of histidase (Q), urocanase (R) and IPPAnase (S) in the sagittal mouse brain slice using avidin-biotin-peroxidase complex staining assay. Cb: cerebellum; VMH: ventromedial hypothalamic nucleus; PMV: premammillary nucleus, ventral part; PnC, pontine reticular nucleus; AHA, anterior hypothalamic, anterior; NAc, nucleus accumbens; Hpc, hippocampus; CC, cingulate cortex.

(T) *In situ* hybridization for urocanase on cerebellum, frontal cortex and HPC slices from adult mouse brain.

(U) Western blot analysis of urocanase, IPPAnase and FTCD in synaptosomes. PSD-95 as the marker of synaptosomes.

(V and W) The normalized intensities of intracellular UCA, IPPA, FMGA and GLU in neurons from HPC of mice after intracerebroventricular (ICV) injection of glycyl-glycine (GG) (2.6 μg, 1 μl) or saline (1 μl). These mice received intra-HPC injection of AAV-shRNA against urocanase (0.5 μl/side, 1.3×10^{12} vg/ml) (V) or random control shRNA (shRandom, 0.5 μl/side, 1.6×10^{12} vg/ml) (W) 3 weeks before single-cell MS tests. vg, vector genomes. All data were normalized to their respective controls (ICV saline group).

(X-BB) Effects of ICV injection of GG on the basic electrophysiological properties of HPC neurons. The resting membrane potential (X), resistant input (Y), action potential amplitude (Z), action potential threshold (AA) and action potential frequency (BB) of neurons in HPC slices from mice after ICV injection of GG (2.6 μg, 1 μl) and saline (1 μl).

(CC–II) Immunocytochemical examination of NeuN-positive neurons in different brain regions after 2-h ICV injection of GG. (CC-HH) Sample photomicrographs of NeuN staining from saline-treated (left) and GG-treated (right) mice. Five brain regions were exhibited and the NeuN+ neurons were counted in the field of view (FOV, 300 μm x 300 μm). Scale bar = 100 μm. (II) Cell counting of NeuN+ neurons displayed no difference between saline-treated and GG-treated mice in the above regions. Th: thalamus; HT: hypothalamus; Au1: primary auditory cortex; S1: primary sensory cortex.

(JJ and KK) Effects of ICV injection of GG on intracellular level of metabolites related to neuronal health (JJ) and other GLU biosynthetic pathway (KK) in HPC neurons. The normalized intensities of intracellular ATP, pyruvate, GLN and GABA in single neurons from the HPC of mice after ICV injection of GG (2.6 μg, 1 μl) or saline (1 μl). All data were normalized to their respective controls (ICV saline group).

(LL–NN) Representative MS/MS spectra of HIS (LL), UCA (MM) and GLU (NN) in single HPC neurons with or without preincubation of HIS (0.2 mg/ml, 1 h) or GG (0.13 mg/ml, 2 h).

(OO and PP) Representative MS/MS spectra of UCA (OO) and GLU (PP) in single HPC neurons with or without preincubation of UCA (0.7 mg/ml, 20 min) or GG (0.13 mg/ml, 80 min).

All digits within the columns represent numbers of total neurons measured from 3 mice. Data are represented as mean ± SEM. $^{**}p < 0.01$, $^{***}p < 0.001$, ns, not significant ($p > 0.05$) based on unpaired t test.

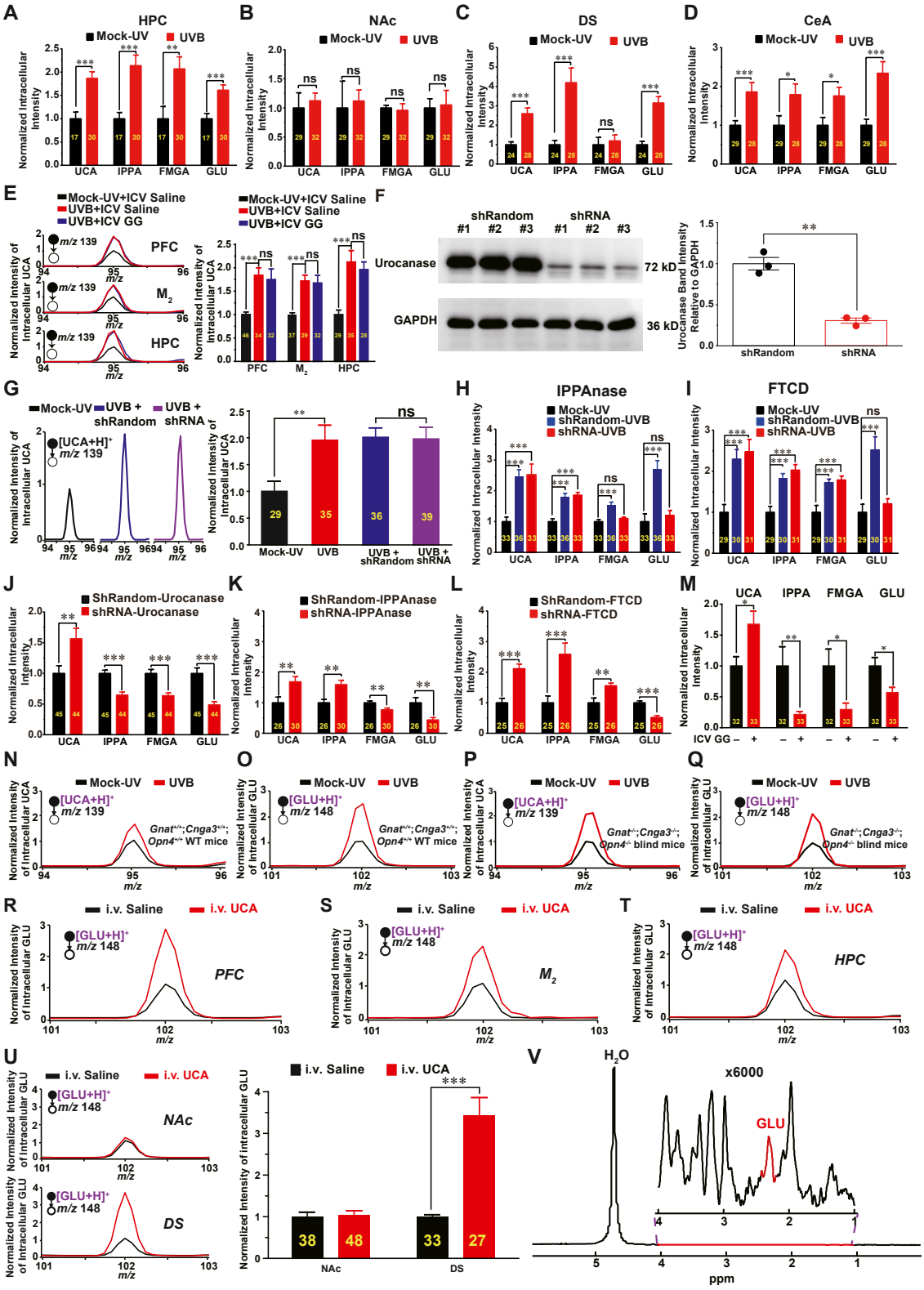

Figure S4. Effects of UVB Exposure and i.v. UCA on UCA-GLU Pathway in the Brain, Related to Figure 4

(A–D) Effects of UVB exposure on intracellular levels of metabolites involved in UCA-GLU pathway, including UCA, IPPA, FMGA and GLU, in single HPC (A), NAc (B), DS (C) and CeA (D) neurons. All data were normalized to their respective controls (mock-UV groups).

(legend continued on next page)

(E) Representative MS/MS spectra (Left) and normalized intensities (Right) of intracellular UCA in single neurons of PFC, M_2 and HPC of mice with or without mock-UV treatment, UVB exposure or ICV injection of GG (2.6 μg, 1 μl). Data were normalized to their respective controls (mock-UV groups without ICV injection of GG).

(F) Knockdown efficacy of urocanase shRNA constructs. The western blot (Left) and normalized band intensity (Right) of urocanase in HEK293T cells, which were treated by the lentiviral short hairpin RNAs against urocanase (shRNAs, 0.5 μl/side, 10^9 TU/ml) or random control shRNA (shRandom, 0.5 μl/side, 10^9 TU/ml).

(G) Representative MS/MS spectra (Left) and normalized intensities (Right) of intracellular UCA showing the effects of intra-HPC injection of lentiviral shRNA against *Uroc1* (shRNA, 0.5 μl/side, 10^9 TU/ml) or random control shRNA (shRandom, 0.5 μl/side, 10^9 TU/ml) on UVB-induced elevation of intracellular UCA level in single HPC neurons. Data were normalized to their respective controls (mock-UV groups).

(H and I) The normalized intensities of intracellular UCA, IPPA, FMGA and GLU in single HPC neurons of mice exposed to UVB or mock-UV. These mice received intra-HPC injection of AAV-shRNA (0.5 μl/side, 1.4×10^{12} vg/ml) against IPPAnase (H) and FTCD (I) or random control shRNA (shRandom, 0.5 μl/side, 1.6×10^{12} vg/ml) 3 weeks before single-cell MS tests. vg, vector genomes. Data were normalized to their respective controls (mock-UV groups).

(J–L) The normalized intensities of intracellular UCA, IPPA, FMGA and GLU in single HPC neurons of mice which received intra-HPC injection of AAV-shRNA (0.5 μl/side) against urocanase (1.3×10^{12} vg/ml) (J) IPPAnase (1.4×10^{12} vg/ml) (K) and FTCD (1.4×10^{12} vg/ml) (L) or random control shRNA (shRandom, 1.6×10^{12} vg/ml) 3 weeks before single-cell MS tests. vg, vector genomes. Data were normalized to their respective controls (shRandom groups).

(M) The normalized intensities of intracellular UCA, IPPA, FMGA and GLU in single neurons from the HPC of mice after ICV injection of GG (2.6 μg, 1 μl) or saline (1 μl). All data were normalized to their respective controls (ICV saline group).

(N–Q) Representative MS/MS spectra of UCA (N and P) and GLU (O and Q) in single HPC neurons of WT (*Gnat*$^{+/+}$;*Cnga3*$^{+/+}$;*Opn4*$^{+/+}$) mice (N and O) and triple knockout (*Gnat*$^{-/-}$;*Cnga3*$^{-/-}$;*Opn4*$^{-/-}$) blind mice (P and Q) after mock-UV (black line) or UVB (red line) exposure. All spectra were normalized to their respective controls (mock-UV group).

(R–T) Representative MS/MS spectra of intracellular GLU in single neurons from brain regions of PFC (R), M_2 (S) and HPC (T) after i.v. UCA (20 mg/kg, 30 min, red line) or saline (black line).

(U) MS/MS spectra (Left) and normalized intensities (Right) of intracellular GLU in single neurons from NAc and DS of mice with i.v. injection of UCA (20 mg/kg, 30 min) or saline. All data were normalized to i.v. saline group.

(V) *In vivo* ^{1}H MR spectra with (inset) and without water suppression, acquired from the M_2 region in mice brain. GLU signal is highlighted (red) in blow-up spectra. All digits within the columns represent numbers of total neurons measured from 3 mice. Data are represented as mean ± SEM. *$p < 0.05$, **$p < 0.01$, ***$p < 0.001$, ns, not significant ($p > 0.05$) based on unpaired t test.

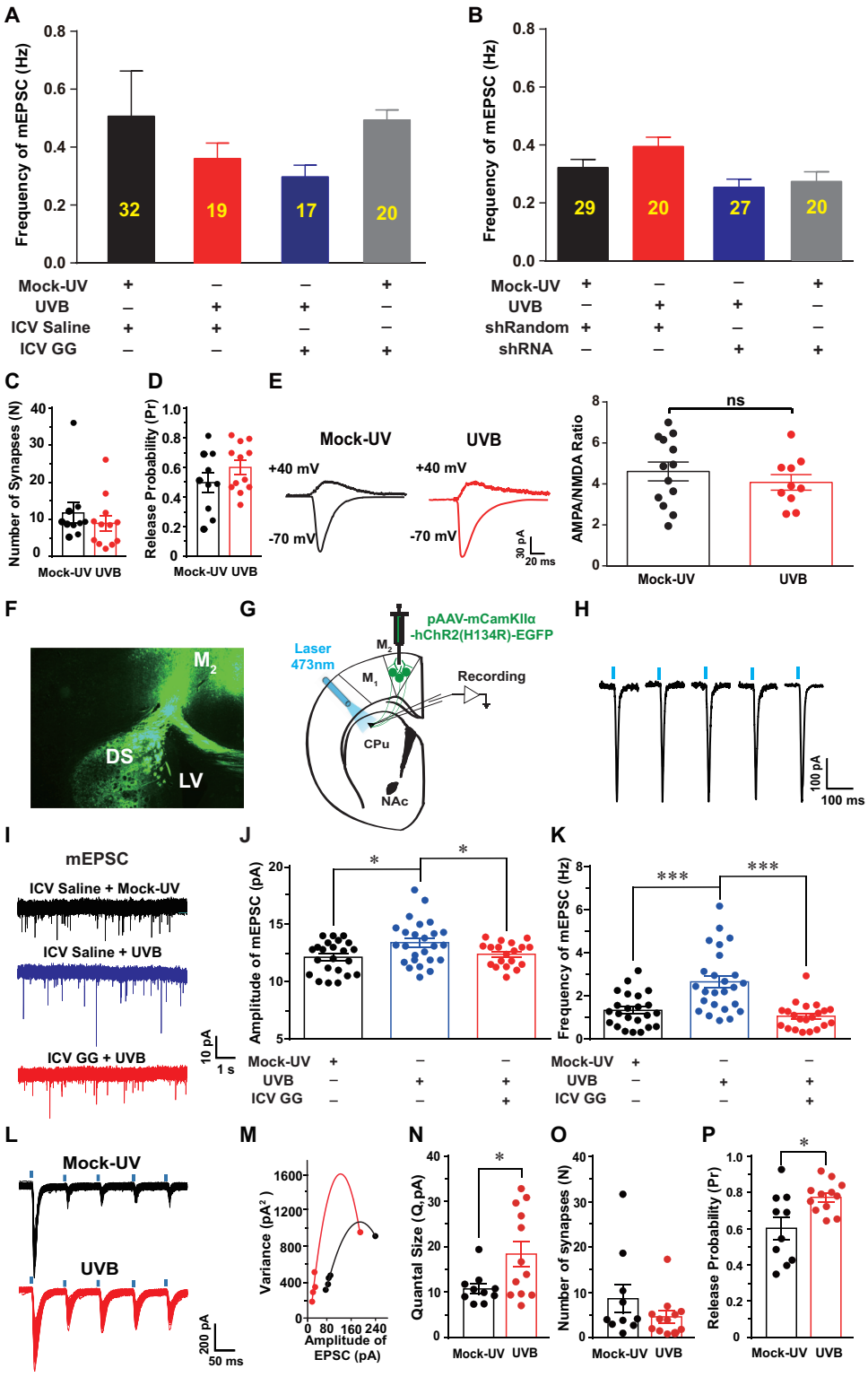

Figure S5. Effects of UVB Exposure on Glutamatergic Synaptic Transmission from HPC CA3 to CA1 and from M_2 to DS, Related to Figure 5

(A) Quantitative frequency of mEPSCs of CA1 neurons from mice with or without mock-UV, UVB exposure and ICV injection of GG (2.6 μg, 1 μl).

(B) Quantitative frequency of mEPSCs of CA1 neurons from mice with or without mock-UV, UVB exposure and intra-HPC CA3 injection of AAV-shRNA (0.5 μl/side, 1.3 × 10^{12} vg/ml) against urocanase or random control shRNA (shRandom, 0.5 μl/side, 1.6 × 10^{12} vg/ml). vg, vector genomes.

(C and D) Effects of UVB exposure on number of synapses (N) (C) and release probability (Pr) (D).

(legend continued on next page)

(E) Effects of UVB exposure on the ratio between AMPA and NMDA receptor contribution to EPSCs. (Left) Sample traces representing EPSCs recorded while holding cells at negative (−70 mV) and positive (+40 mV) membrane potentials. (Right) The ratio of amplitudes of the NMDA EPSC to those of the AMPA EPSC in neurons of HPC of mice receiving mock-UV or UVB exposure.

(F–P) Effects of UVB exposure on glutamatergic synaptic transmission from M_2 to DS. (F) Representative image showing the viral expression of pAAV-mCamKIIα-hChR2(H134R)-EGFP along the neuronal projection from M_2 to DS. (G) Schematic image showing the electrophysiological recording of DS neurons with optical stimulation of $GLU^{M2\rightarrow DS}$ projecting fibers. (H) Trace records of blue light (473 nm, 5 ms) evoked EPSC in DS neurons. Neurons responding to optical stimulation were selected for the following recordings (J-P). (J-L) The trace records (I), quantitative amplitudes (J) and frequencies (K) of mEPSCs of DS neurons from mice with or without mock-UV (black dots, n = 23 neurons from 3 mice), UVB exposure (blue dots, n = 25 neurons from 3 mice) or ICV injection of GG (red dots, 2.6 μg, 1 μl, n = 21 neurons from 3 mice). (L-P) A combination of optogenetic stimulation and MPFA allows the measurement of circuit-specific synaptic properties. (L) EPSCs were triggered by optical stimulation of $GLU^{M2\rightarrow DS}$ neuronal fibers. Example traces of 100 overlap synaptic responses from mice exposed to mock-UV or UVB. (M) MPFA of the example recordings in (L). (N and O) Quantal parameters quantal size (N) and number of synapses (O) were derived from the parabolic fit of the variance-mean analysis (mock-UV: n = 10 neurons from 3 mice; UVB: n = 12 neurons from 3 mice). (P) The release probability (Pr) was calculated according to Equation 1 in star methods.

All digits within the columns represent numbers of total neurons measured from 3 mice. Data are represented as mean ± SEM. *$p < 0.05$, ***$p < 0.001$, ns, not significant ($p > 0.05$) based on unpaired t test.

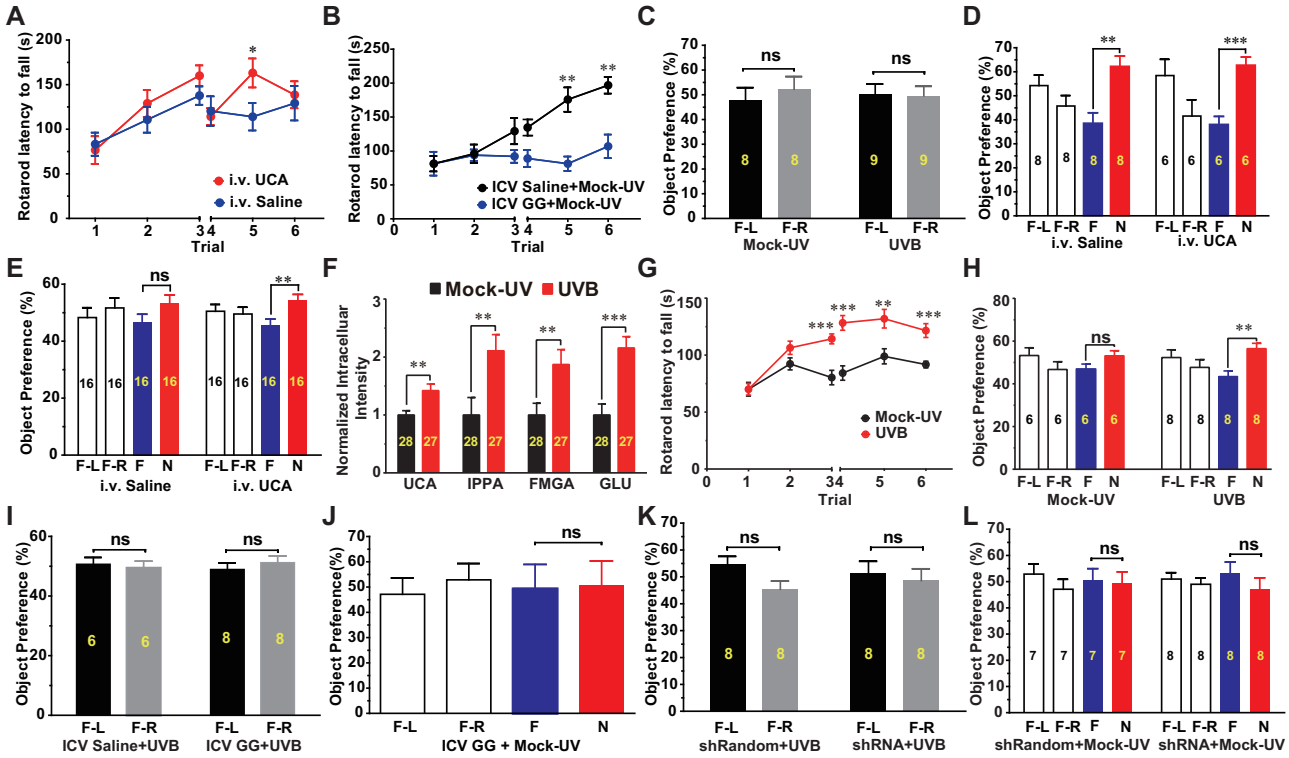

Figure S6. Effects of UVB Exposure on Rotarod Learning and Object Recognition Memory in Male and Female Mice, Related to Figure 6

(A)Time spent on the rotarod in the mice with i.v. injection of UCA (20 mg/kg, 30 min, red dots, N = 10 mice) or saline as control (blue dots, N = 11 mice).

(B)Time spent on the rotarod in the mice with ICV administration of GG (13.2 μg, 1 μl, blue dots, N = 5 mice) or saline as control (black dots, N = 13 mice) followed by mock-UV exposure.

(C) The preference on familiar objects placed on different sites (F-L: familiar objects on the left side; F-R: familiar objects on the right side) during 3-min familiarization in two groups of mice, which were arranged to receive mock-UV or UVB exposure 24 h after familiarization.

(D) The preference of mice on familiar and novel objects during 3-min test at 2 h after familiarization. Mice received i.v. injection of UCA (20 mg/kg, 30 min) or saline before test. F-L: familiar objects on the left side; F-R: familiar objects on the right side.

(E) The preference of mice on familiar and novel objects during 3-min test at 24 h after familiarization. Mice received i.v. injection of UCA (20 mg/kg, 30 min) or saline before test. F-L: familiar objects on the left side; F-R: familiar objects on the right side.

(F–H) Effects of UVB exposure on hippocampal intracellular UCA-GLU metabolic pathway and neurobehaviors of female mice. (F) Normalized MS intensities of intracellular UCA, IPPA, FMGA and GLU in single neurons of HPC of female mice exposed to mock-UV or UVB. Data were normalized to their respective controls (mock-UV groups). All digits within the columns represent numbers of total neurons measured from 3 mice. (G) Latency to fall on the accelerating rotarod for each trial on days 1 and 2 in mice after mock-UV (black dots, N = 10 mice) or UVB (red dots, N = 14 mice) exposure. (H) The preference of female mice to familiar and novel objects during a 3-min test at 24 h after familiarization. Mice received mock-UV (N = 6 mice) or UVB exposure (N = 8 mice) for 2 h before the test. F-L: familiar objects on the left side; F-R: familiar objects on the right side; N: novel objects.

(I) The preference on familiar objects placed on different sites (F-L: familiar objects on the left side; F-R: familiar objects on the right side) during 3-min familiarization in two groups of mice, which were arranged to receive ICV injection of GG (13.2 μg, 1 μl) or saline followed by UVB exposure 24 h after familiarization.

(J) The preference on familiar and novel objects during 3-min test at 24 h after familiarization. Mice received ICV injection of GG (13.2 μg, 1 μl) followed by Mock-UV exposure. F-L: familiar objects on the left side; F-R: familiar objects on the right side.

(K) The preference on familiar objects placed on different sites (F-L: familiar objects on the left side; F-R: familiar objects on the right side) during 3-min familiarization in two groups of mice, which were arranged to receive intra-HPC CA3 injection of *Uroc1* shRNA (0.5 μl/side, 10^9 TU/ml) or shRandom (0.5 μl/side, 10^9 TU/ml) followed by UVB exposure before test.

(L) The preference on familiar and novel objects during 3-min test at 24 h after familiarization. Mice received intra-HPC CA3 injection of *Uroc1* shRNA (0.5 μl/side, 10^9 TU/ml) or shRandom (0.5 μl/side, 10^9 TU/ml) followed by mock-UV exposure. F-L: familiar objects on the left side; F-R: familiar objects on the right side.

All digits within the columns represent the numbers of total neurons measured from 3 mice or the numbers of mice in each group. Data are represented as mean ± SEM. *p < 0.05, **p < 0.01, ***p < 0.001, ns, not significant (p > 0.05) based on unpaired t test.